7 Multidirectional water flow, sediment transport, erosion, and deposition

Introduction

Water currents that periodically reverse direction are associated with (1) water surface waves formed by the wind; (2) tidal waves caused by the gravitational attractions between the Earth, Moon, and Sun; and (3) tsunami waves caused by earthquakes, landslides, volcanic eruptions, and meteorite impacts. Temporal and spatial variation in the velocity and direction of these currents is complicated. These waves undergo fundamental changes as they move into shoaling water and towards land, further modifying the associated currents. These waves also normally act together in the sea, and it is common for unidirectional currents to be superimposed upon the wave currents. For example, the wind that acts on the water surface to produce wind waves also drags surface water in the general direction of the wind. Therefore, water currents associated with these various types of waves are truly multidirectional. Reviews of wind waves, tidal waves, and associated water currents and sediment transport are given by Defant (1958), J. R. L. Allen (1970, 1985), Komar (1976, 1998), Bowden (1983), Pond and Pickard (1983), Sleath (1984), Fredsoe and Deigaard (1992), Nielsen (1992), and P. A. Allen (1997). Reviews of tsunamis and their effects on the Earth include Iida and Iwasaki (1983), Mader (1988), Dawson (1994, 1999), Shiki *et al.* (2000), Bryant (2001), and Satake (2005). Wind waves and associated wind-drag currents will be discussed first, then tidal waves, and finally tsunami waves.

Definitions

The parameters and symbols used to represent wave geometry and movement are given in Table 7.1 and Figure 7.1. Water-surface waves can be classified using their period (the time taken for one wavelength to pass a point) and the forces responsible for forming them. *Wind waves* have periods ranging from a fraction of a second to 300 seconds (but mainly within the range 1–20 seconds) and are generated by the wind acting on the water surface. Wind waves are called *sea waves* when the wind is actively working on the water surface to generate waves, *swell waves* when they travel beyond the influence of the wind, and *surf waves* when they break on the shore. A further important classification of water-surface waves is based on their wavelength relative to undisturbed water depth:

$L/d < 2$	deep-water waves
$2 < L/d < 20$	intermediate-water waves
$L/d > 20$	shallow-water waves

Tidal waves have periods of about 12.5 hours (semidiurnal), 25 hours (diurnal), and longer. Tides are generated by gravitational forces and modified by the Coriolis force and friction. Since the wavelength of a semidiurnal tidal wave is half of the circumference of the Earth, and the mean oceanic depth is about 4 km, a tidal wave is a shallow-water wave. *Tsunami waves* result from isolated events such as submarine earthquakes, volcanic eruptions, and landslides. They have periods of minutes and lengths up to 500 km, and are shallow-water waves. Other kinds of water-surface waves include those formed when water is periodically driven against shorelines by the wind, temporarily increasing water level at the coast (e.g., storm surges at sea, or *seiches* in lakes: Chapter 14). Internal waves along density interfaces within water bodies related to spatial variations in salinity, temperature, or suspended sediment concentration are discussed in Chapters 14, 15, and 18.

Generation of wind waves

When sustained wind blows over the water surface, wind waves develop, with heights, wave lengths, and periods

TABLE 7.1. Wave parameters

Parameter	Units	Symbol
Wave height	m	H
Water-surface elevation above a datum	m	h
Wave amplitude	m	A
Wave length	m	L
Wave-number ($=2\pi/\lambda$)	m^{-1}	k
Wave period	s	T
Radian frequency ($=2\pi/T$)	s^{-1}	σ
Wave celerity ($=\lambda/T$)	$m\ s^{-1}$	c
Undisturbed water depth	m	d
Orbital diameter of an Airy wave	m	d_o
Orbital velocity	$m\ s^{-1}$	u

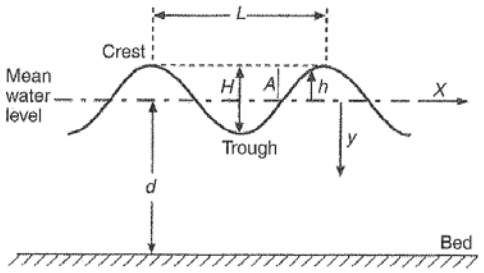

FIGURE 7.1. Definition of wave parameters

controlled by the wind velocity, duration of wind, and distance over which the wind blows (*fetch*). Exactly how wind waves are formed is not fully understood (Allen, 1985; Komar, 1998). Turbulent wind shear acting on the water surface drags water in the direction of the wind and also causes undulations in the water surface. According to the Bernouilli equation (Chapter 5), a wavy water surface causes differences in dynamic air pressure between the crest (low pressure) and the trough (high pressure), tending to increase the wave height. However, turbulent wind pressure acting normal to the water surface also influences wave geometry, and is necessary to create waves. The result is that a range of various wave sizes and speeds is formed in the generation area. In view of the incomplete understanding of wave generation, most attempts to predict wave parameters from wind velocity, duration, and fetch have been empirical (e.g., Carter, 1982; Komar, 1998). However, recent models for predicting wave parameters from wind data (e.g., NOAA's WAVEWATCH III: http://polar.ncep.noaa.gov/waves/) utilize theoretical models for wave generation and dispersion, and perform well when the results are compared with data from buoys and satellite altimetry.

As sea waves leave the generation area, the waves with the longest periods travel the fastest (called *dispersion*: see Equation (7.5)). Also, viscous damping affects short-period waves preferentially. Therefore, complex sea waves become transformed into groups of waves with similar geometry and speed, and these regular swell waves can travel for thousands of kilometers across entire oceans. Waves generated by storms off Antarctica can reach the coast of Alaska. Changes that wind waves undergo as they move into shallow water and approach shorelines are described below.

Measurement and analysis of wind waves

Temporal variations in water-surface elevation associated with waves are recorded using a variety of techniques, involving hydrostatic pressure or acoustic sensors attached to the bed, electronic wave staffs on fixed platforms, buoys that measure water-surface slopes and accelerations, and reflection of radar or laser beams from satellites or aircraft. Wave speed and direction are calculated from pairs of measurements of water-surface elevation, and measured using current meters. Time series of wave parameters are likely to be complicated, because any one storm will generate a large variety of waves, and the waves arriving at a point may have been generated by different storms in different areas. It is normal to calculate the mean and variance of wave height, maximum wave height, and significant wave height (the mean height of the highest third of waves). There are many more complicated ways of analyzing time series (e.g., autocorrelation, spectral analysis: see the appendix). Simple statistical analysis of 40,000 observations of wave height (Komar, 1976) reveals that 45% of waves are less than 1.2 m high, 80% are less than 3.6 m high, and 90% are less than 6 m high. The largest wind wave ever recorded was about 34 m high. The reliability of direct observations of the largest waves can be questioned for obvious reasons. Indeed, larger waves have occurred, but most observers did not survive to report them. However, much more wave data has become available since the advent of remote sensing of the ocean surface. Most common wave periods are 1–10 seconds, and storm wave periods are typically 10–15 seconds.

Wave theories

Wave theories attempt to explain the relationship between the geometry and kinematics of simple

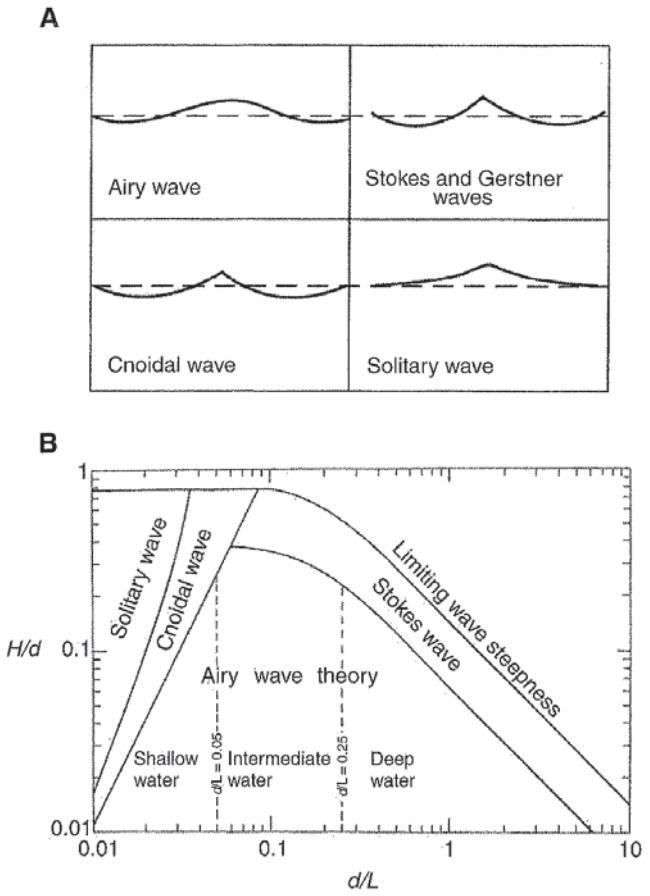

FIGURE 7.2. (A) Theoretical wave forms in profile. (B) Regions of applicability of wave theories. Modified from Komar (1998).

idealized waves and the water motions associated with them. These theoretical approaches involve simplifying the basic equations of motion (e.g., conservation of mass and momentum) in order to obtain analytical solutions. The more simplifications made, the simpler the theory. The four main theories and their ranges of applicability in terms of H/d and L/d are shown in Figure 7.2. The theories, in order of increasing mathematical complexity, are Airy, Stokes, Gerstner, and cnoidal. In addition to these analytical approaches to understanding wave mechanics, it is now possible to solve the equations of motion directly using numerical methods and fast, powerful computers. The Airy and Stokes wave theories are simple enough for this book, and give important insights into the nature of wave currents. These theories assume that the flow is nonviscous, irrotational, and two-dimensional, and that there are no superimposed unidirectional currents.

Airy's linear theory of oscillatory waves is called the small-amplitude theory, because it applies to waves with small amplitude (height) relative to depth (Figure 7.2). It is called a linear theory because it considers only the first-order terms in the series expansion of the equations of motion. The idealized wave profile is sinusoidal, and given by

$$h = A\sin(kx - \sigma t) \tag{7.1}$$

where h is the water-surface elevation above or below the average, undisturbed water level at a given point in space and time, A is the wave amplitude (half of the wave height), $k = 2\pi/L$, where L is the wave length, x is the distance in the direction of wave motion, $\sigma = 2\pi/T$, where T is the wave period, and t is time (Table 7.1 and Figure 7.1). General equations for wave celerity (speed) and wavelength are

$$c^2 = (g/k)\tanh(kd) \tag{7.2}$$

$$c = (g/\sigma)\tanh(kd) \tag{7.3}$$

$$L = [gT^2/(2\pi)]\tanh(kd) \tag{7.4}$$

where tanh is hyperbolic tangent. For *deep-water waves*, kd is large, and $\tanh(kd)$ tends to 1 for large kd. Therefore, the celerity and wave length of deep-water waves are

$$c = \sqrt{(g/k)} = g/\sigma \tag{7.5}$$

$$L = gT^2/(2\pi) \tag{7.6}$$

Equation (7.5) is a wave-dispersion equation because it describes how waves with the largest wave length travel with the greatest speed, allowing waves of different lengths to be dispersed as they travel away from their generation region. For *shallow-water waves*, kd is small and $\tanh(kd)$ tends to kd, so

$$c = \sqrt{(gd)} \tag{7.7}$$

$$L = T\sqrt{(gd)} \tag{7.8}$$

With small-amplitude theory, water particles beneath a translating wave describe *closed orbits* (Figure 7.3), and the theory predicts the velocity of the water particles in these orbits. The fact that the water particles are not translated with the wave form can be appreciated by watching an object floating on the water surface as a wave passes. For *deep-water waves*, the orbits are circular, with diameter d_o equal to wave height H at the water surface. Since water particles complete one orbit in one wave period, the velocity of the orbital motions at the water surface u_s is $\pi H/T$. However, the orbit diameters decrease exponentially downwards for deep-water waves according to

$$d_o = H\exp(-ky) \tag{7.9}$$

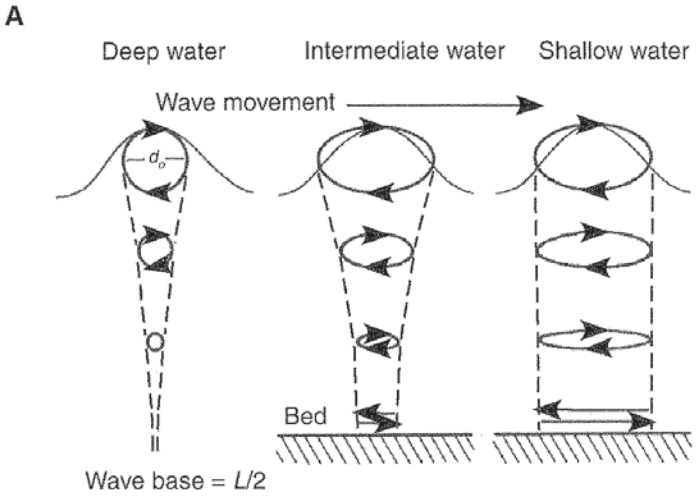

FIGURE 7.3. (A) Airy-wave theory: water-particle orbits for deep-, intermediate-, and shallow-water waves. (B) Water-particle trajectories for intermediate-water waves photographed over one wave period. Trajectories are almost circles at the upper surface, but are progressively flatter ellipses with decreasing long axis towards the bed. Trajectories are not completely closed. The wave amplitude is 0.04 times the wave length, and the depth is 0.22 times the wave length. From Van Dyke (1982).

where y is the distance below the undisturbed water level. At $y = L/2$, the orbital diameter is only 4% of its surface value, and the orbital velocity is considered to be negligible. This level is called *wave base*. Since $d > L/2$ for deep-water waves, the bed is always below wave base, and the bed does not interact with the orbital water motions. For intermediate-water waves, the orbits are ellipses with horizontal long axes that decrease in length with depth (Figure 7.3). For *shallow-water waves*, the orbits are ellipses that become flatter with depth but their long-axis lengths are constant (Figure 7.3).

The maximum near-bed horizontal velocity during an orbit is given as

$$u_{max} = \pi H/T \sinh(kd) \tag{7.10}$$

where sinh is hyperbolic sine. For deep-water waves, $\sinh(kd)$ increases as kd increases, such that u_{max} tends to zero, as expected. For shallow-water waves, $\sinh(kd)$ tends to kd as kd decreases. Therefore, the maximum near-bed orbital velocity is given as

$$u_{max} = Hc/(2d) = H\sqrt{(gd)}/(2d) \tag{7.11}$$

A shallow-water wave with a height of 0.4 m in water 5 m deep would have a maximum near-bed water velocity of about 0.3 m s^{-1}, easily enough to entrain fine-grained sand.

Directions of orbital water motion are related to the wave form (Figure 7.3). Water motion is in the direction of wave advance under the wave crest, but in the opposite direction under the trough. Upward components of water motion occur beneath the side of the wave facing the direction of wave advance, because the water level increases as the wave crest approaches. Downward components of water motion occur beneath the opposite side of the wave because the water level decreases as the trough approaches. As the wave form advances, so do the directions of water motion. In the case of intermediate-water waves, the near-bed water motions have a vertical component but are mainly horizontal and reversing in direction. Near-bed water motions for shallow-water waves are dominantly horizontal and reversing. The maximum near-bed horizontal water velocity in the direction of wave motion is underneath the wave crest, whereas that in the opposite direction is underneath the wave trough.

The implications of these near-bed flow patterns for sediment transport are given below.

Progressive waves have potential energy by virtue of the existence of crests and troughs, and kinetic energy by virtue of the motion of water beneath the waves. The total wave energy (kinetic and potential) per unit water-surface area is $0.5\rho g A^2$, and the wave power per unit width of wave crest is the product of wave energy per unit area and wave celerity.

Stokes' finite-amplitude theory takes into account second-order terms in the series expansion of the equations of motion, and the effects of finite wave height. This theory predicts that the orbits are not actually closed (Figure 7.2B) and there is a non-periodic drift of fluid in the direction of wave motion throughout the flow depth, due to the fact that orbital velocities under wave crests (in the direction of wave motion) are slightly greater than those under wave troughs (opposite to the direction of wave motion). As orbital diameters of deep-water waves decrease exponentially downwards, so do the drift velocities. This relationship is not applicable to waves in shallow water, where orbital diameters do not decrease downwards exponentially, and the effects of friction on net drift must be accounted for. Furthermore, if the waves are moving towards a solid boundary such as cliffs or a beach, continuity of water mass requires a return flow of equal mass. Theoretical flow-velocity distributions throughout the flow depth for Stokes non-periodic drift for various wave conditions (and including viscous effects; Longuet-Higgins (1953)) are shown in Figure 7.4. In all cases, there is a net drift at the bed in the direction of wave motion. However, there are many uncertainties about the veracity of these theoretical drift velocities. This is because prediction of drift velocities must also take into account the effects of drift due to surface wind shear (e.g., geostrophic currents), and the coastal circulation system involving edge waves and rip currents (see below). Introduction of viscosity into Stokes' theory results in a bottom boundary layer, the thickness of which equals the square root of $\mu T/(\pi\rho)$. This oscillatory boundary layer is a few millimeters thick for large waves, and may be laminar or turbulent. The transition from laminar to turbulent occurs as the orbital diameter at the bed (and hence the water velocity) increases.

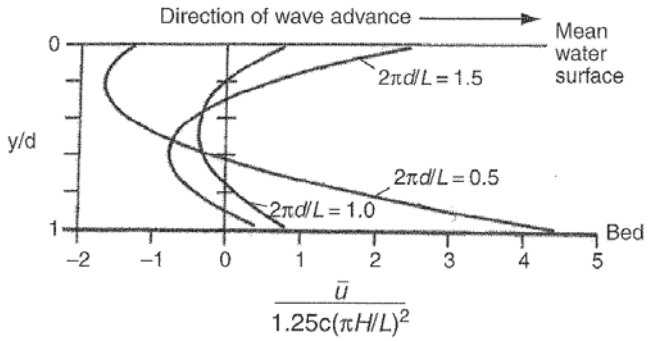

FIGURE 7.4. The theoretical vertical variation of the time-averaged drift velocity (dimensionless) in a laboratory channel for Stokes waves of various depth/wave length ratios. Modified from Longuet-Higgins (1953) by Komar (1998).

Another important result of Stokes' theory is a criterion for *wave breaking*. This occurs when the two faces of the wave make an angle of 120° at the crest, and the water velocity at the crest just equals the wave celerity. If the water velocity exceeds the wave speed, water overtakes the wave and the wave starts to break. The condition for breaking is

$$H/L = 0.142 \tanh(kd) \tag{7.12}$$

which for shallow-water waves (small kd) leads to

$$H/L = 0.142(kd) \quad \text{or} \quad H = 0.89d \tag{7.13}$$

Most waves would break when the wave height was less than this theoretical criterion. Measurements of H/d at wave-breaking range from 0.7 to 1.3, with larger values for steeper bed slopes (Paul Komar, personal communication).

Wind waves in shoaling water

Changes in wave form and speed

As wind waves move into progressively shallower water, wave celerity and wave length decrease (Equations (7.7) and (7.8)), wave height increases, the crests become more peaked while the troughs broaden (trochoidal shape), the waves become progressively more asymmetrical in profile, and they ultimately become oversteepened and break (Figure 7.5). In the absence of geostrophic currents and rip currents (see below), the magnitude and degree of asymmetry of near-bed currents (due to non-periodic drift) increase up to the point of breaking as the water depth decreases and wave height increases (Figure 7.5). The nature of wave breaking depends on the bed steepness (Figure 7.6). For low-angle beds, water gradually spills down the wave front and the wave height gradually decreases (a *spilling breaker*). As the bed steepness increases, a coherent mass of water from the crest plunges downwards, enclosing a tube or barrel (surfer

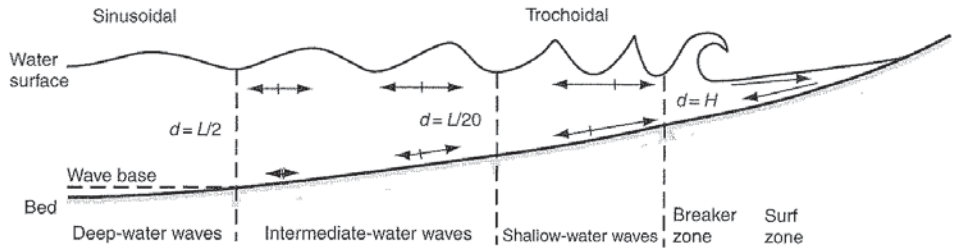

FIGURE 7.5. Waves and associated water currents in shoaling water. Waves change from long, low, symmetrical, and sinusoidal to short, high, asymmetrical, and trochoidal as the depth decreases. Arrows indicate the maximum orbital velocity under a wave trough or crest. Just above wave base, the maximum near-bed orbital velocity is small and of the same magnitude in either direction (Stokes drift is minimal). As waves change with decreasing depth, the near-bed orbital velocity increases, and the onshore velocity under the wave crest increases relative to the offshore velocity under the trough (due to Stokes drift). Near the water surface, the water velocity under wave crests and troughs increases onshore as waves increase in height. Differences between onshore- and offshore-directed flow velocities are due to Stokes drift. Arrows in the surf zone indicate swash and backwash.

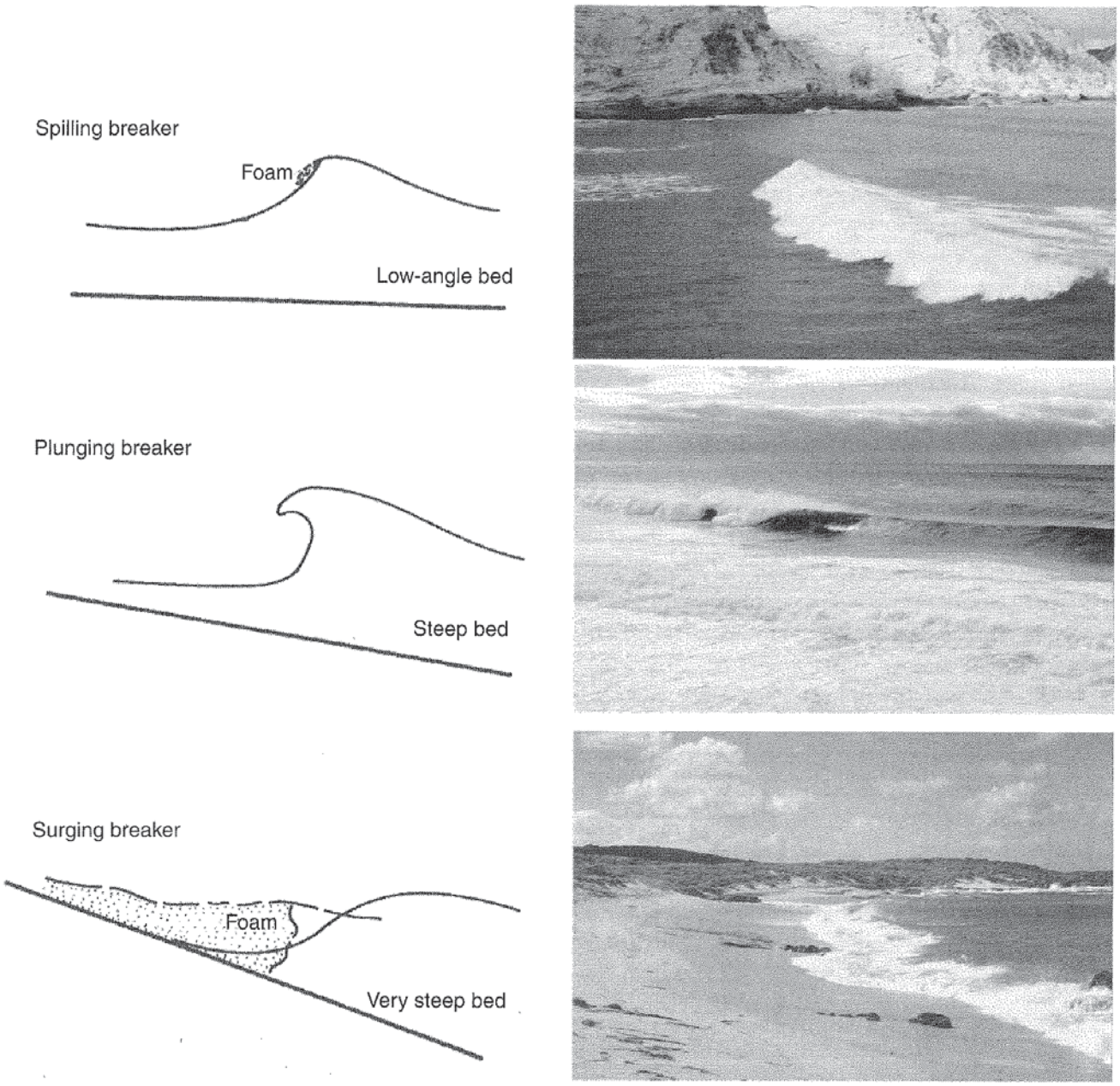

FIGURE 7.6. Types of breaking waves, depending on bed slope and wave steepness. Photos of breakers courtesy of Rob Brander.

term) of air (a *plunging breaker*). With very steep beds, the base of the wave surges up the beach before the wave can break (a *surging breaker*). The *surf zone* is landward of the *breaker zone*, the rush of water up the beach following wave breaking is called the *swash*, and the return flow is called the *backwash*. The water velocity in the surf zone following wave breaking is directly proportional to the maximum near-bed orbital velocity at the point of breaking. The relatively elevated water surface in the surf and swash zones (Figure 7.5) is called the *wave set-up*, and is due to the momentum flux of the breaking waves.

Wave reflection, refraction, and diffraction

Waves can be reflected, refracted, or diffracted as they approach a shoreline (Figure 7.7), and these phenomena can be treated in a similar way to light waves. Waves are reflected from cliffs and steep beaches, with the angle of reflection equal to the angle of incidence. The incident and reflected waves interact to give a pattern of distinct wave crests in different directions. If the angle of incidence is 0° (wave crests parallel to the shoreline), the incident and reflected waves interact to form *standing waves*. The profile of a standing Airy wave can be obtained by adding the wave-profile equations (e.g., Equation (7.1)) for waves of a given geometry moving in opposite directions, resulting in

$$h = 2A\sin(kx)\sin(\sigma t) \tag{7.14}$$

The amplitude of the standing wave is double that of the individual waves. The streamline pattern for standing waves (Figure 7.8) shows that the near-bed flow direction reverses each wave period, but the maximum horizontal velocity occurs at the points where the water level does not change (*nodes*). The points that experience the maximum range of water level (*antinodes*) are associated with vertical (up and down) water motions only. Net drift associated with standing waves (Figure 7.8) gives rise to a convergence of near-bed flow within the boundary layer towards the nodes.

Wave refraction can be treated using Snell's law, in which the ratio of the sine of the angle between the wave crest and the topographic contours to the wave celerity is constant. Therefore, because the wave celerity decreases as depth decreases (Equation (7.7)), the angle that wave crests make with topographic contours also decreases with depth (Figure 7.7). This causes wave crests to become progressively closer to parallel to linear shorelines, to bend towards headlands, and to

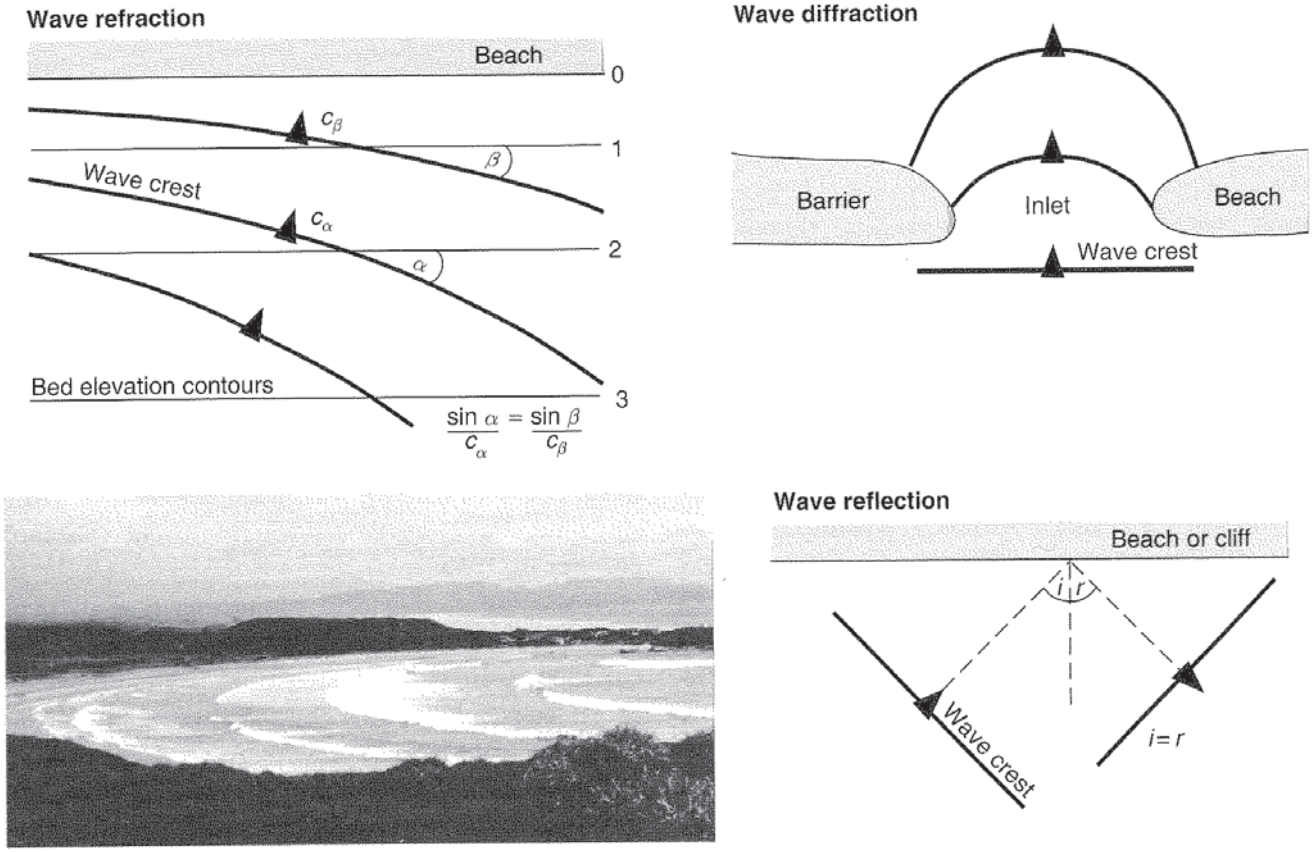

FIGURE 7.7. Explanation of wave reflection, refraction, and diffraction. A photo of wave-crest curvature by refraction in a New Zealand bay. From Hyndman and Hyndman (2006).

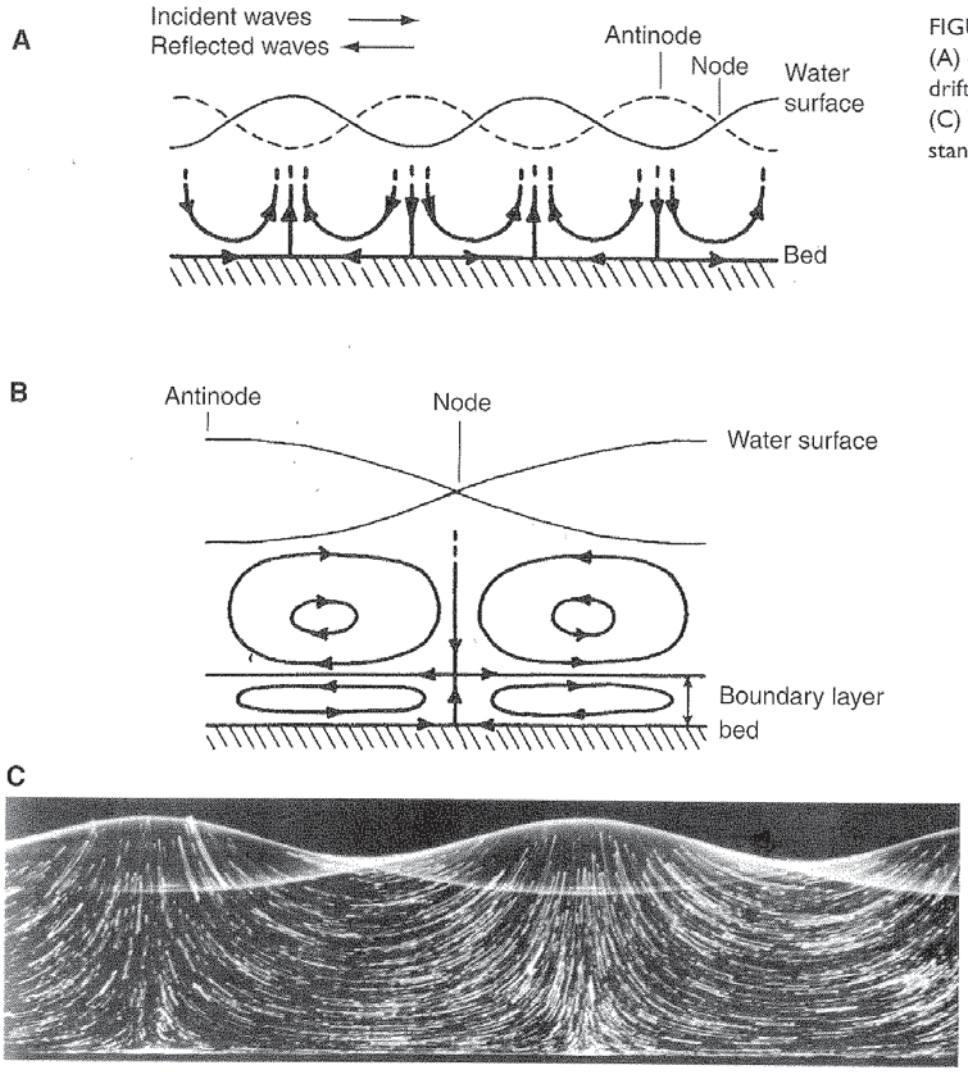

FIGURE 7.8. Standing waves: (A) oscillatory currents and (B) net drift (modified from Allen (1985)). (C) Water-particle trajectories under standing waves. From Van Dyke (1982).

bend away from submarine channels (Figure 7.7). Typical patterns of wave diffraction are shown in Figure 7.7.

Rip currents and nearshore circulation

Rip currents are localized unidirectional currents that originate in the breaker zone and flow offshore for tens to hundreds of meters (Figure 7.9). These currents are meters wide, and may be channelized near the breaker zone, where flow velocities may be on the order of several m s^{-1}. They spread laterally, decelerate, and dissipate offshore. The velocity and distance of offshore water movement increase with incoming wave height. Rip currents are spaced regularly along the shoreline, with a mean spacing of tens to hundreds of meters. They occur where breaking waves have relatively low height. Breaking waves between rip currents have relatively large height. This difference in breaking-wave height results in alongshore variation in water level in the surf zone (*wave set-up*), resulting in alongshore water flow towards the sources of the rip currents (Figure 7.9). This water flow in the surf zone follows a zig-zag path due to swash and backwash. Therefore, there is a pattern of water circulation in the near-shore zone that involves net shoreward drift associated with shoaling waves, alongshore drift in the surf zone, and offshore motion in rip currents (Shepard and Inman, 1950).

In the case of oblique wave approach, the pattern of near-shore circulation is modified (Figure 7.9). Rip currents are directed obliquely offshore, and the longshore currents in the surf zone become unidirectional but spatially periodic in velocity. As the angle of wave approach increases, rip currents cease to exist, and wave-generated currents in the surf zone are dominantly alongshore. The velocity of these longshore currents increases with the angle of wave approach and the

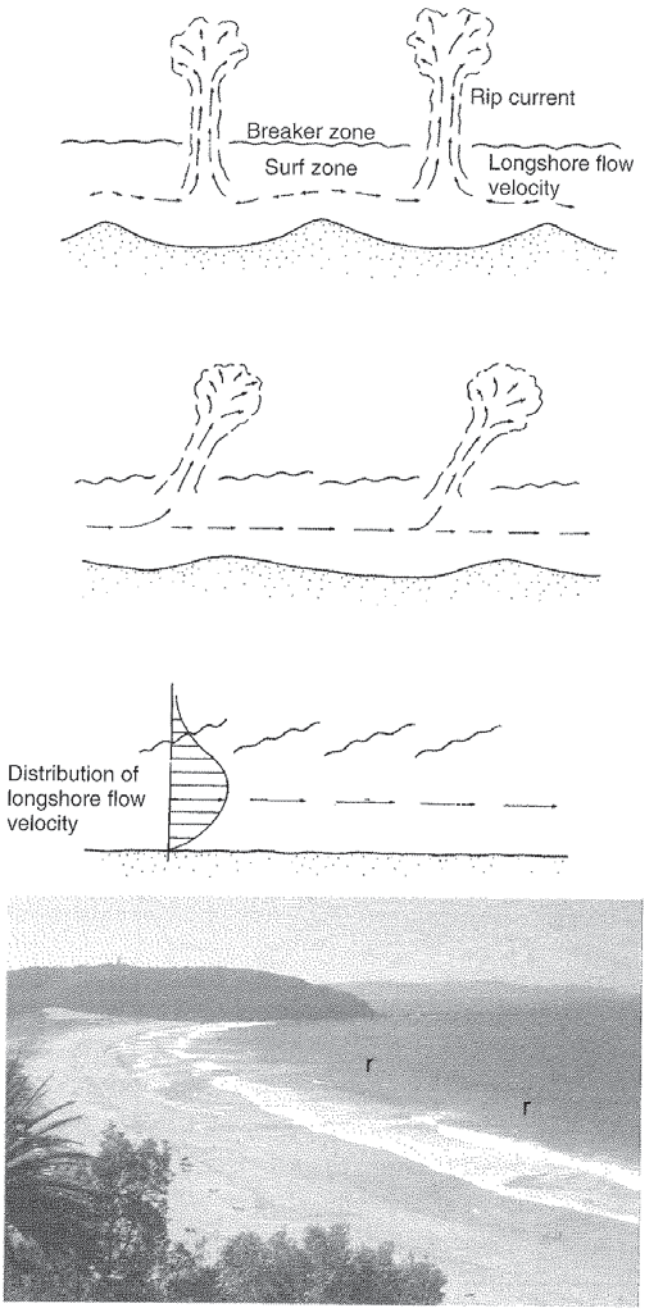

FIGURE 7.9. Nearshore water circulation involving net drift below incoming waves, longshore currents in the surf zone, and rip currents. The angle of wave approach increases from the top diagram to the bottom diagram. The length of arrows is proportional to the flow velocity. Modified from Komar (1998). The photo (courtesy of Rob Brander) shows rip currents (r) cutting through the breaker zone.

maximum orbital velocity at breaking (which increases with breaker height), and can reach several $m\,s^{-1}$. Net alongshore drift gives rise to shoreline features such as spits (discussed in Chapter 15).

This alongshore variation in wave set-up, nearshore water circulation, and specifically the regular spacing of rip currents probably owes its origin to standing *edge waves*, with their crestlines approximately normal to the shoreline (e.g., Bowen, 1969; Bowen and Inman, 1969; Huntley and Bowen, 1973; Guza and Davis, 1974; Guza and Bowen, 1975; Huntley *et al.*, 1981; Holman, 1983; Oltman-Shay and Guza, 1987). Progressive edge waves are due to refraction of oblique reflected waves back towards the shoreline, and this process requires a relatively steep bed slope and/or adjacent cliffs. The amplitude of these waves decreases exponentially offshore. The wave length of edge waves is proportional to the square of the wave period, and also increases slightly with bed slope. The period of edge waves can be the same as that of the incoming waves, but edge waves can also have a range of different lengths and periods. So-called subharmonic edge waves have periods that are twice those of the incident waves. It is quite possible that edge waves of the same period can be moving in opposite directions, thus producing standing edge waves. When the crest of a standing edge wave coincides with the crest of a breaking wave, the combined wave will have a large height, and the water level in the surf zone after breaking will be relatively high (Figure 7.10). The coincidence of this wave crest and the trough of the edge wave will give rise to low waves and low water level in the surf zone. Rip currents occur where incoming wave crests coincide with edge-wave troughs, and the spacing of rip currents equals the edge-wave length.

If rip currents form channels, the increased water depth over the channel will result in wave refraction (Figure 7.7), resulting in divergence of wave paths away from the channel and reinforcing the distribution of high and low waves due to edge waves. The near-shore circulation associated with edge waves also probably gives rise to regularly spaced ridges and troughs on beaches, called *beach cusps* (discussed in Chapter 15).

Wind shear and geostrophic currents

Wind acting on the water surface of the ocean and large lakes not only forms waves: it also drags surface water (up to a depth of about 100 m) in the general direction of the wind. The interaction of these wind-drag or wind-shear currents with wind-wave currents results in a complex current pattern, especially near coasts and on continental shelves. Therefore, it is difficult to understand sediment transport, erosion, and deposition by wind waves without also considering the associated wind-shear currents. Wind-shear currents in major oceans follow the major patterns of wind circulation (associated with polar easterlies, mid-latitude

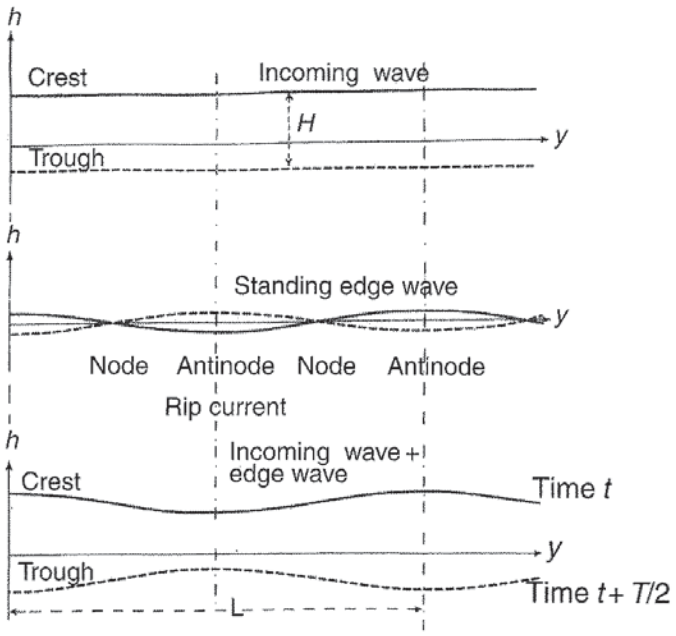

FIGURE 7.10. Addition of an incoming wave and a standing edge wave at the breaker zone, giving longshore variation in breaker height and wave set-up. The breaker height is greatest where the edge wave and incoming wave are in phase, and lowest where they are 180° out of phase. Rip currents occur where the breaker height and wave set-up are lowest. Modified from Komar (1998).

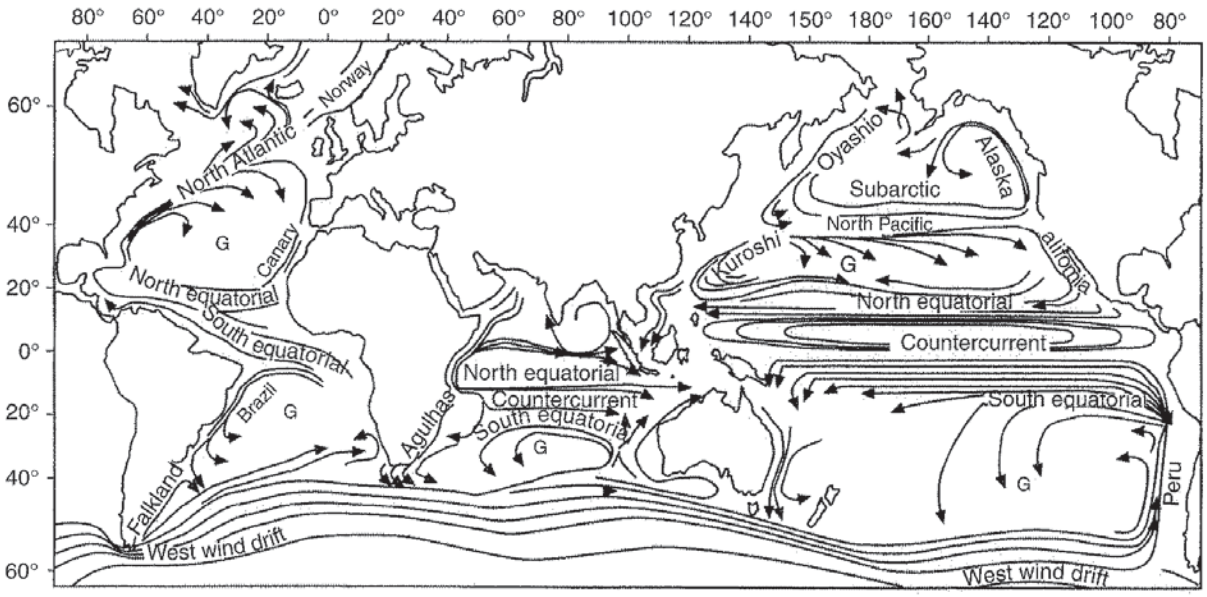

FIGURE 7.11. Global wind-drift surface currents, drawn as streamlines such that closer streamlines indicate stronger currents; G indicates subtropical gyre. From Leeder (1999).

westerlies, and tropical trade winds: Figure 7.11). These currents are deflected by the Coriolis force and by continents, giving rise to ocean-scale circulations that are clockwise in the northern hemisphere and anticlockwise in the southern hemisphere. An example is the Gulf Stream that transports warm Caribbean water to the shores of western Europe, having a major impact on the climate.

Wind-shear current velocities vary from a few centimeters per second to meters per second. Current velocity and direction depend on the velocity of the wind, the distance below the water surface, the depth of water, the latitude, and the proximity to land masses. Current velocity decreases downwards in the water body (a surface boundary layer exists) because of the viscosity of water. Surface-water currents are deflected relative to the wind direction by the Coriolis force, which is given by

$$F_c = m2V\Omega \sin\phi \tag{7.15}$$

where m is mass, V is the flow velocity, Ω is the angular velocity of the Earth's rotation (equal to 2π divided by 23 hours and 56 minutes, or 7.23×10^{-5} radians per second), and ϕ is latitude. Progressive deflection of water currents by the Coriolis force with increasing depth gives rise to so-called *Ekman spirals* (Figure 7.12). Ekman

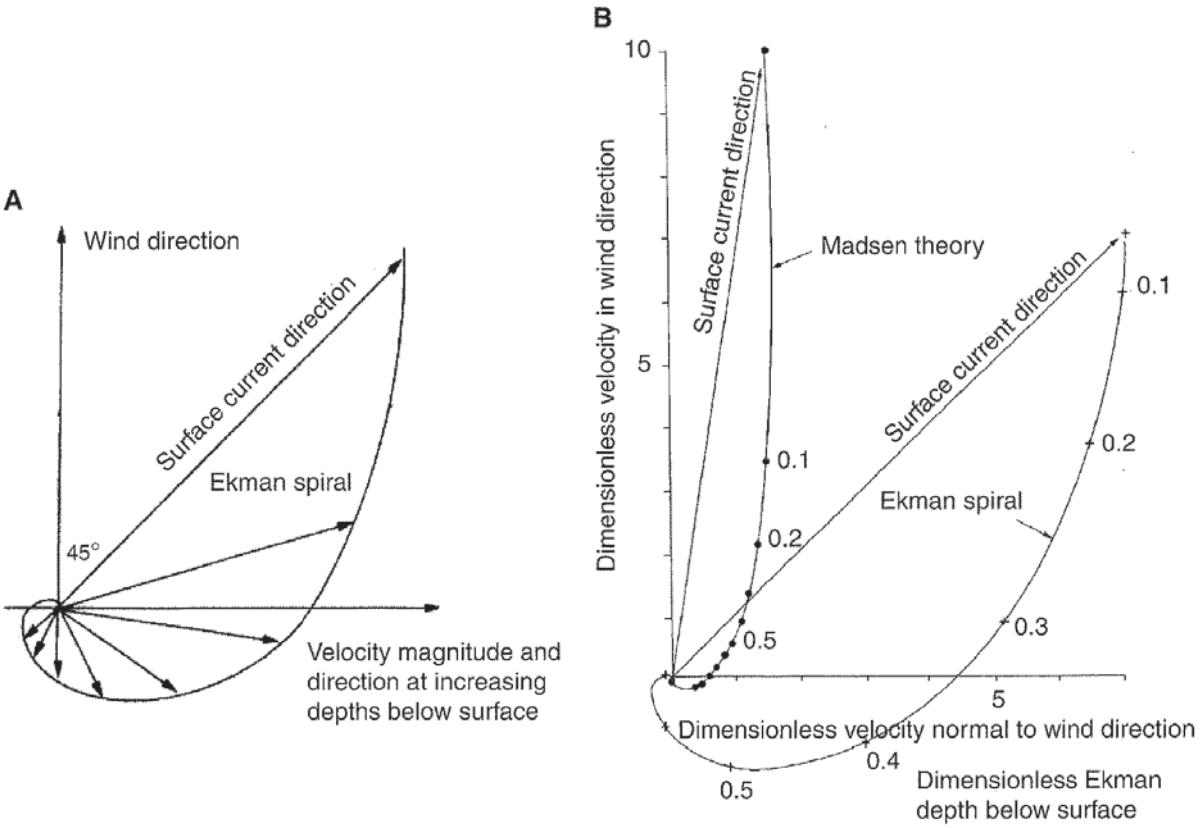

FIGURE 7.12. (A) A plan view of an Ekman spiral (for the northern hemisphere), showing how the magnitude and direction of velocity change with distance below the water surface. (B) A comparison of the variations of orthogonal velocity magnitudes with the distance below the water surface as predicted by Ekman and Madsen theories. Modified from Allen (1997).

spirals are predicted from the balance among wind shear, fluid friction, and the Coriolis force, assuming that there is no water-surface slope and no friction at the bed, and that the wind is steady and prolonged. This theoretical force balance gives expressions for the depth variation of flow velocity and direction, and for the depth at which currents become negligible (the *Ekman depth*, which is also the point at which there is a small velocity opposite to the surface velocity). Ekman theory predicts that the surface-water current should make an angle of 45° to the surface wind direction, and that the current velocity decreases exponentially downwards from the water surface.

Observations do not agree well with Ekman theory (Madsen, 1977; Keen and Glenn, 1994; Allen, 1997). The angle between the directions of the wind and surface currents is commonly less than 10° (Figure 7.12), and the surface-water currents are commonly about 3% of the wind velocity measured 10 m above the water surface, i.e.

$$V_s \approx 25u_* = 25(\rho_a/\rho_w)w_* \tag{7.16}$$

where V_s is the surface current velocity, u_* is the water shear velocity, w_* is the wind shear velocity, and $\rho_a/\rho_w = 0.035$ is the ratio of the densities of air and water. The wind shear velocity is given as

$$w_* = W\sqrt{C_d} \tag{7.17}$$

where W is the wind velocity at 10 m above the water surface and C_d is a drag coefficient that depends on the wind velocity, and is on the order of 10^{-3}. The thickness of the Ekman layer is given by

$$L_E = 96w_*/\sin\phi \tag{7.18}$$

Therefore, the velocity of a surface-water current and the thickness of the Ekman layer, for a wind velocity of 10 m s^{-1} at latitude 65°, are, using Equations (7.16)–(7.18) and $C_d = 0.0014$, 0.33 m s^{-1} and 39.6 m, respectively. In Madsen's analysis, the velocity decreases with depth more rapidly than predicted by Ekman (Figure 7.12). Actually, surface currents will normally be due to both wind shear and wave-induced Stokes drift, and the latter may be up to half of the velocity of the surface current. Also, bed friction greatly modifies Ekman spirals in shallow water (above the Ekman depth), as discussed below.

Wind-shear currents commonly result in changes in the elevation of the water surface, one example being

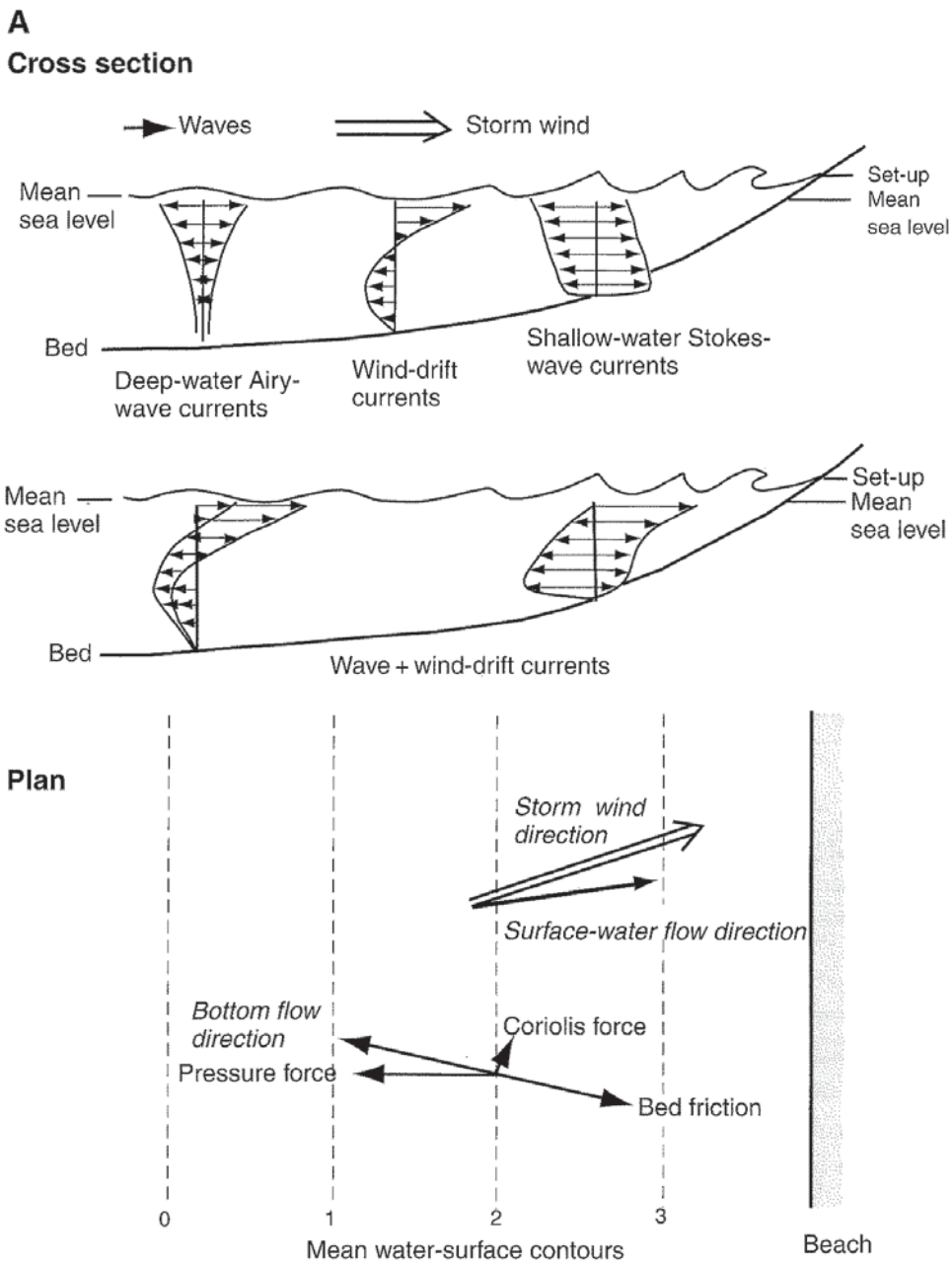

FIGURE 7.13. Idealized combined wave currents and wind-drift currents near a coastline in the northern hemisphere for (A) onshore wind, (B) offshore wind, and (C) alongshore wind. Cross-sections show wind-drift currents and the maximum horizontal component of wave-induced currents under wave troughs or crests, and combined currents. The length of arrows is proportional to the water velocity. Plans show water-surface contours and directions of wind-drift currents at various levels in the flow. The directions of wind-drift currents are determined by the direction and magnitude of the pressure (arising from the water-surface slope), friction, and Coriolis forces. Bottom currents are strongly influenced by bed friction.

when there is a component of water flow towards a land mass. A wind-shear current will obviously have an onshore component if the wind has an onshore component. However, an alongshore wind may also produce an onshore surface flow because of the Coriolis deflection of the surface water. The obstruction to flow causes a rise in water level at the coast, called a *wind set-up* or a *storm tide* (Figure 7.13), and an offshore-directed water-surface slope. The wind set-up at the coast may be calculated by balancing the pressure gradient arising from the sloping water surface, the wind shear stress, and the bed shear stress arising from water motion. This force balance is given as

$$\tau_w - \tau_b = \rho g(d+e)S \tag{7.19}$$

where τ_w and τ_b are the wind shear stress and bed shear stress, respectively, ρ is the fluid density, g is the gravitational acceleration, $d+e$ is the sum of the water depth and super-elevation of the water surface, and S is the water-surface slope in the direction of the shear stresses. If the super-elevation e is small relative to the water depth, Equation (7.19) can be simplified to

$$\tau_w = C\rho g d S \tag{7.20}$$

where C varies from 1 to 1.5. The set-up due to wind shear may be added to by the breaking of large waves (wave set-up), and by the effects of low atmospheric pressure (as in the center of a depression). The set-up may be several meters above normal mean sea level

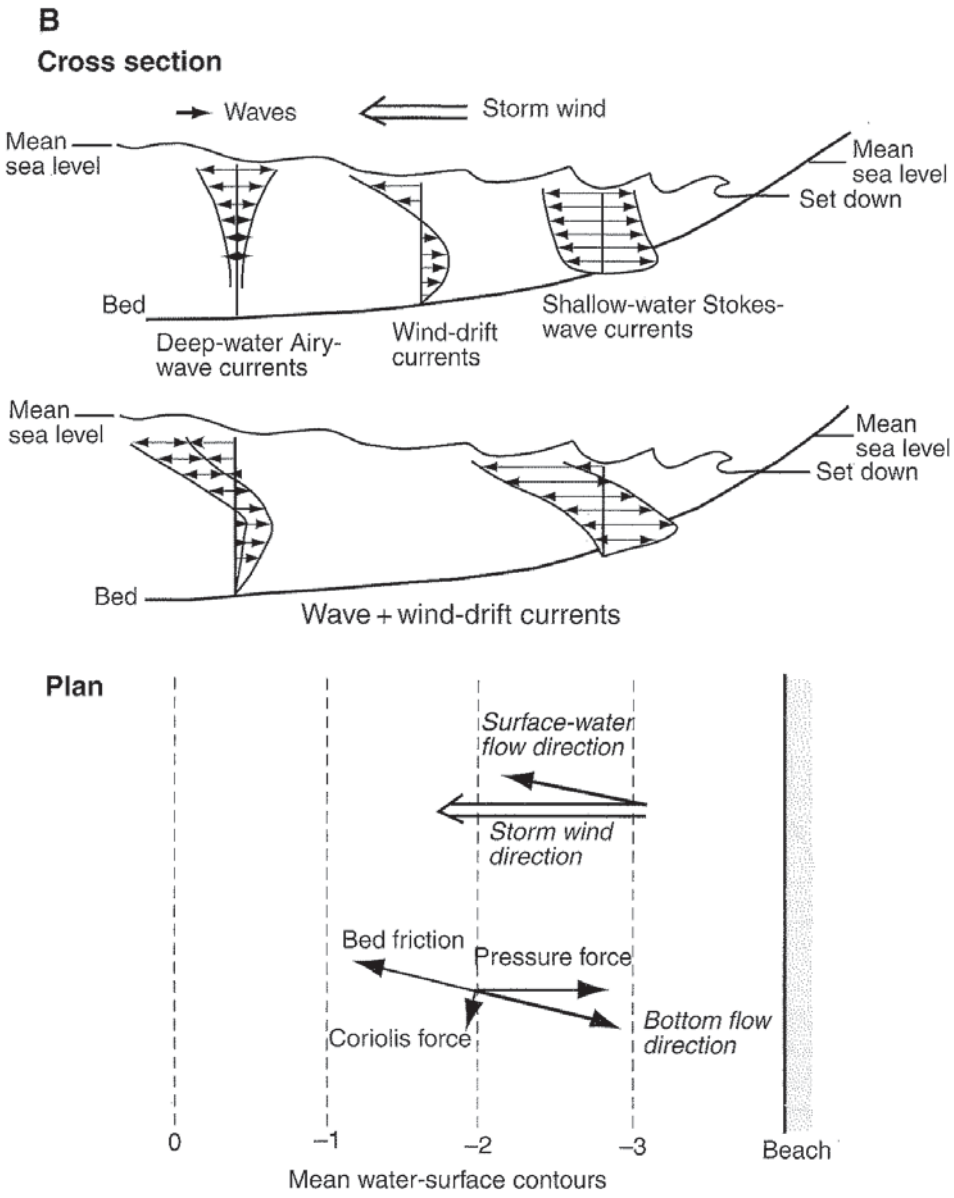

FIGURE 7.13. Continued.

during major storms. Large set-ups combined with high tides can produce devastating flooding of coastal regions. If a wind-shear current has an offshore component, there is a *set-down* at the coast, and an onshore-directed water-surface slope.

Continuity of water mass requires that the onshore movement of water in wind-shear currents (plus wave-induced drift) is balanced by an offshore movement of the same mass of fluid. This offshore movement is in the form of a unidirectional bottom current that flows down the pressure gradient. During major storms, such bottom currents can reach velocities of meters per second, decreasing in velocity offshore (due to increasing depth and decreasing water-surface slope). Such strong currents can easily cut channels in the sea bed. Offshore-directed return flows that are normal to the shoreline at the coast may be subsequently deflected by the Coriolis force, until the Coriolis force is exactly balanced by the pressure gradient (Figure 7.13), assuming that bed friction is ignored. Currents caused by pressure gradients and turned by the Coriolis force in the absence of bed friction are called *geostrophic currents*. Geostrophic means Earth-turned. However, the near-bed, offshore-directed flows must be influenced by bed friction as discussed below.

The influence of frictional resistance at the bed on wind-drift currents must be considered in shallow water, above the Ekman depth. A reduction in wind-shear flow velocity near the bed due to bed friction results in a reduction in the Coriolis force, and this results in a reduction in the angular deviation of the bottom flow from the surface flow. In very shallow

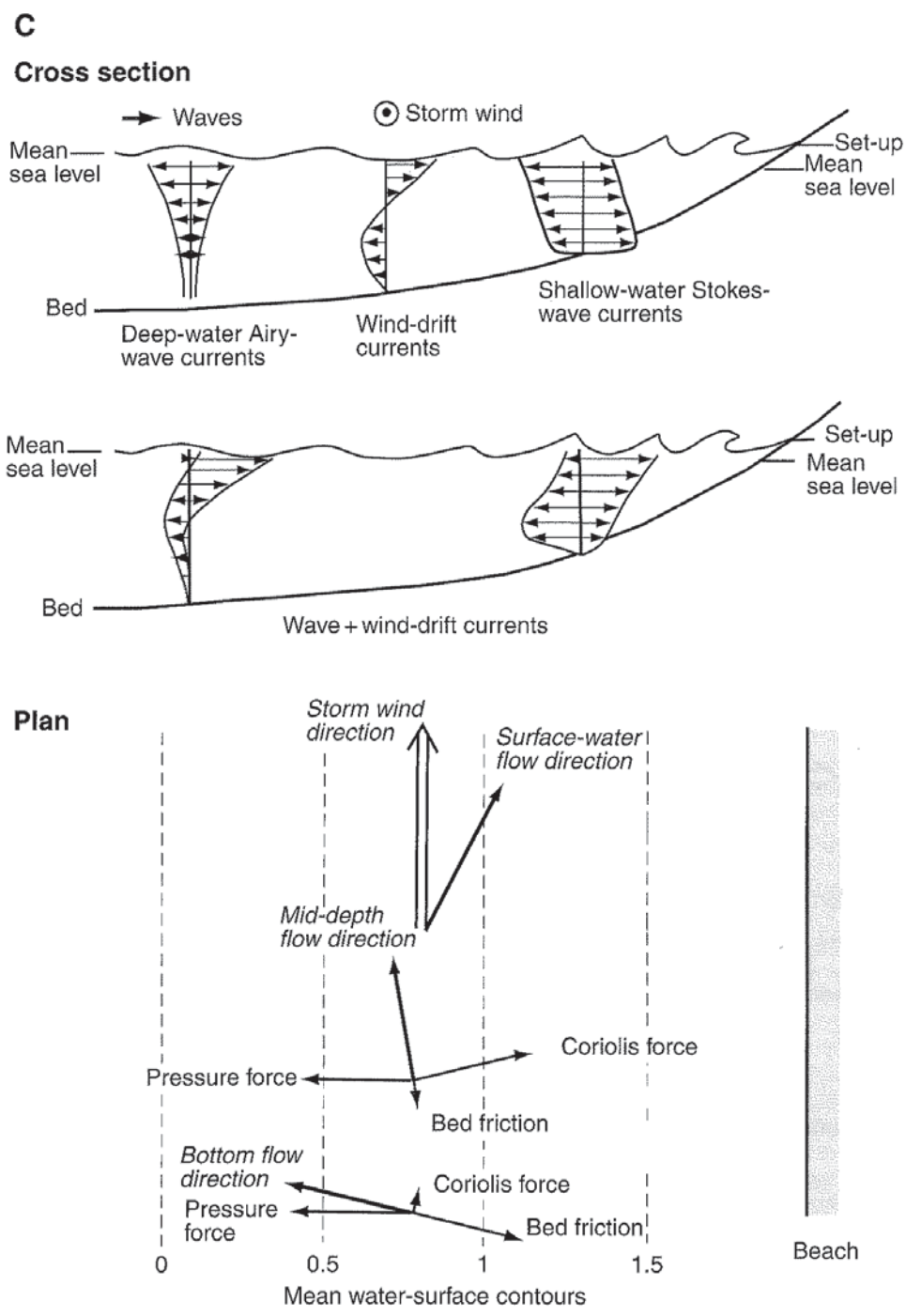

FIGURE 7.13. Continued.

water (0.1 times the Ekman depth, say), the upper Ekman spiral and the bottom layer interact such that the net fluid transport is close to the wind direction. In the case of offshore-directed return flows, the lower regions should always be strongly influenced by bed friction, resulting in a bottom-flow direction very close to the water-surface slope, which is normal to the shoreline (Figure 7.13): compare with Swift *et al.* (1986) and Duke *et al.* (1991).

Wind-shear and geostrophic currents can greatly modify the currents associated with waves (oscillatory motion, net drift, rip currents, longshore currents), producing combined, multidirectional currents. It is therefore probable that current patterns in shallow seas will be very complicated during major storms, when most erosional and depositional activity occurs. Figure 7.13 shows idealized, near-coastal, combined wind-shear and wave-induced currents for various wind directions for the northern hemisphere. The exact nature of these combined currents will depend on the relative magnitudes and directions of wind-shear and wave-induced currents, which are dependent upon wind magnitude

and direction, swell-wave characteristics, sea-bed topography, and so on. In the case of an onshore wind-shear component, the bottom flow varies in velocity with wave period but is mainly offshore, and relatively weak onshore flow components occur only in shallow water. Surface flow is mainly onshore. Such offshore-directed, spatially decelerating bottom currents are expected to erode beaches and deposit bed-load sediment offshore. In addition, high water levels at beaches may result in washovers (Chapter 15) and deposition landwards of the beach as washover fans. Wind-shear currents with an offshore component and a set-down at the coast have near-bed return currents directed onshore (Figure 7.13). This causes upwelling at the coast. When combined with wave-induced currents, near-bed currents vary in magnitude with wave period, but are mainly directed onshore, with weak offshore currents only in shallow water. Surface currents are dominantly offshore. Such onshore accelerating bottom currents are expected to erode the sea bed and deposit bed-load sediment on the beach, while suspended sediment is transported and deposited offshore. It appears that oscillatory bottom currents occur near coasts only when wind-shear currents are negligible.

Thermohaline currents

Thermohaline currents result from horizontal pressure gradients associated with lateral variations in water temperature and/or salinity (and hence water density). These currents are discussed in Chapters 14, 16, and 18.

Sediment transport by wind waves and associated currents

The threshold of entrainment of cohesionless sediment

The threshold of entrainment of cohesionless sediment by oscillatory wave currents can be treated in essentially the same way as for unidirectional currents, even though wave currents are reversing and there is not a persistent turbulent boundary layer like that in unidirectional flows. The bed shear stress must be expressed in terms of the maximum near-bed orbital velocity using

$$\tau_o = f_w \rho u_{max}^2/2 \qquad (7.21)$$

which requires knowledge of the friction coefficient, f_w. The dimensionless bed shear stress and grain Reynolds number can then be used to predict the threshold of

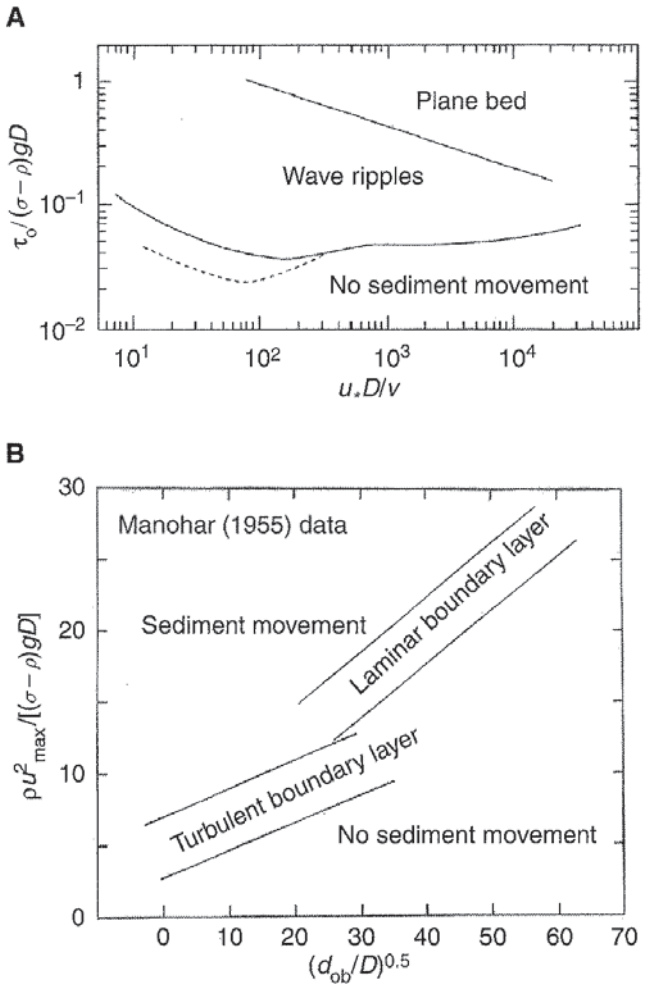

FIGURE 7.14. The threshold of sediment motion under waves based on (A) the dimensionless bed shear stress and grain Reynolds number (modified from Komar and Miller (1975a, b), and (B) the dimensionless maximum near-bed orbital velocity and dimensionless wave orbital diameter (modified from Komar and Miller (1973)). Envelopes of data (from Manohar) are shown for laminar and turbulent boundary layers. The boundary between laminar and turbulent boundary layers is approximately 0.5 mm at the threshold of motion.

motion, as for unidirectional flows (Figure 7.14A). An alternative approach (Komar and Miller, 1973, 1975a; Dingler, 1979; Allen, 1985) is to use a slightly different form of the dimensionless bed shear stress and the ratio of the near-bed orbital diameter, d_{ob}, and mean grain size:

$$\rho u_{max}^2/[(\sigma-\rho)gD] \quad \text{and} \quad d_{ob}/D \qquad (7.22)$$

The form of this relationship depends on the magnitude of d_{ob}/D, which controls whether the boundary layer is laminar (large values) or turbulent (small values) (Figure 7.14B). The transition from laminar to turbulent boundary layer at the threshold of motion occurs at a grain diameter of approximately 0.5 mm. Since u_{max} is a function of the near-bed orbital diameter

and wave period for Airy waves, the threshold of entrainment can be expressed as a function of u_{max}, D, and T for constant sediment density, fluid density, and viscosity. Large storm waves with periods between 10 and 15 seconds are capable of entraining sand in water depths of 100–200 m. However, Airy wave theory is approximate and inappropriate in shallow water. The threshold of motion calculated as above is for mean flow conditions and mean grain size only. Furthermore, it is likely that combined oscillatory and unidirectional currents will be operating at the threshold of grain motion in most natural situations.

Modes and rates of sediment transport

Sand and gravel are transported mainly as bed load, and silt and clay travel mainly in suspension. There have been many more studies of suspended-sediment transport than of bed-load transport by wave currents. Upward-directed water motions associated with gravity waves are known to suspend sediment. The near-bed concentration of suspended sediment increases with orbital velocity, and is dependent on the upward advection of suspended sediment associated with the vortices developed to the lee of ripple crests. Shear turbulence associated with superimposed unidirectional currents can also suspend sediment. However, the intensity of vertical turbulent motions and suspended sediment concentration is much greater in combined flows than in the component flows (Figure 7.15) (Kemp and Simons, 1982; Murray *et al.*, 1991; Osborne and Greenwood, 1993). The concentration of suspended sediment decreases exponentially upwards from the bed both in unidirectional currents and in wave-induced currents.

If there is symmetrical oscillatory water motion affecting the bed, as is the case just above wave base, no net bed-load transport occurs (Figure 7.16). Asymmetrical oscillatory motion near the bed, as is the case for intermediate- and shallow-water waves, produces net bed-load transport in the direction of wave motion as long as the offshore bed slope is not excessive (Figure 7.16). The addition of a unidirectional current to oscillatory currents has a multiplicative effect on the sediment-transport rate rather than an additive effect (e.g., Bagnold, 1963; Grant and Madsen, 1979; Vincent *et al.*, 1982; Green *et al.*, 1990; Murray *et al.*, 1991; Osborne and Greenwood, 1993); see Figures 7.15 and 7.16. This is because the sediment has already been put in motion by the oscillatory currents, and so the unidirectional current can more

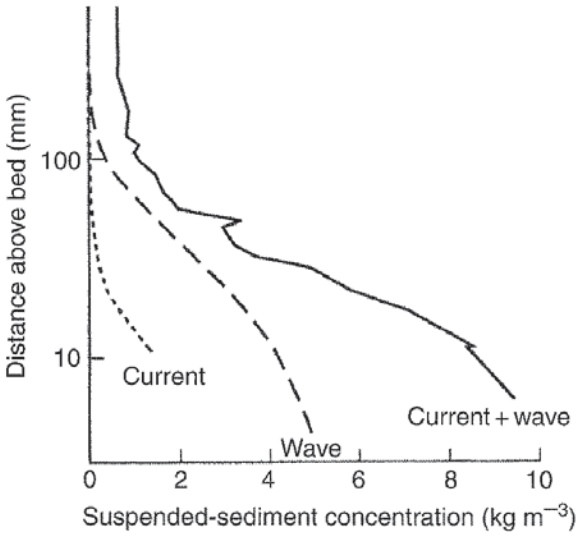

FIGURE 7.15. Experimental vertical variation of the time-averaged suspended sediment concentration for unidirectional current, wave currents, and combined unidirectional and wave currents. Modified from Leeder (1999).

easily transport the sediment. The sediment-transport rate is proportional to the cube of the resultant magnitude of u_{max}. The mean sediment-transport rate of longshore currents associated with oblique wave approach is proportional to the cube of the mean velocity of the longshore current (which is proportional to the maximum near-bed orbital velocity at wave breaking) and also increases with the angle of wave approach. The longshore sediment-transport rate is also proportional to the product of breaker height squared and mean longshore current velocity (Komar, 1998).

Sediment sorting during transport

Since u_{max} increases as water depth decreases and as wave height increases, so also should the mean grain size of the bed load and the suspended load (cf. Chapter 5). The mean grain size of bed load should therefore increase at any point on the sea bed during storms (compared with under fair-weather conditions), and increase from offshore towards the breaker zone. This is actually observed. However, relatively coarse-grained bed sediment occurs on parts of continental shelves where such sediment is not expected to be moved under present-day storm waves. This *relict* sediment was deposited during the last ice age when the sea level was much lower, and most of the continental shelf was a coastal plain traversed by rivers.

As the mean grain size of bed-load sediment increases, the standard deviation of grain size also

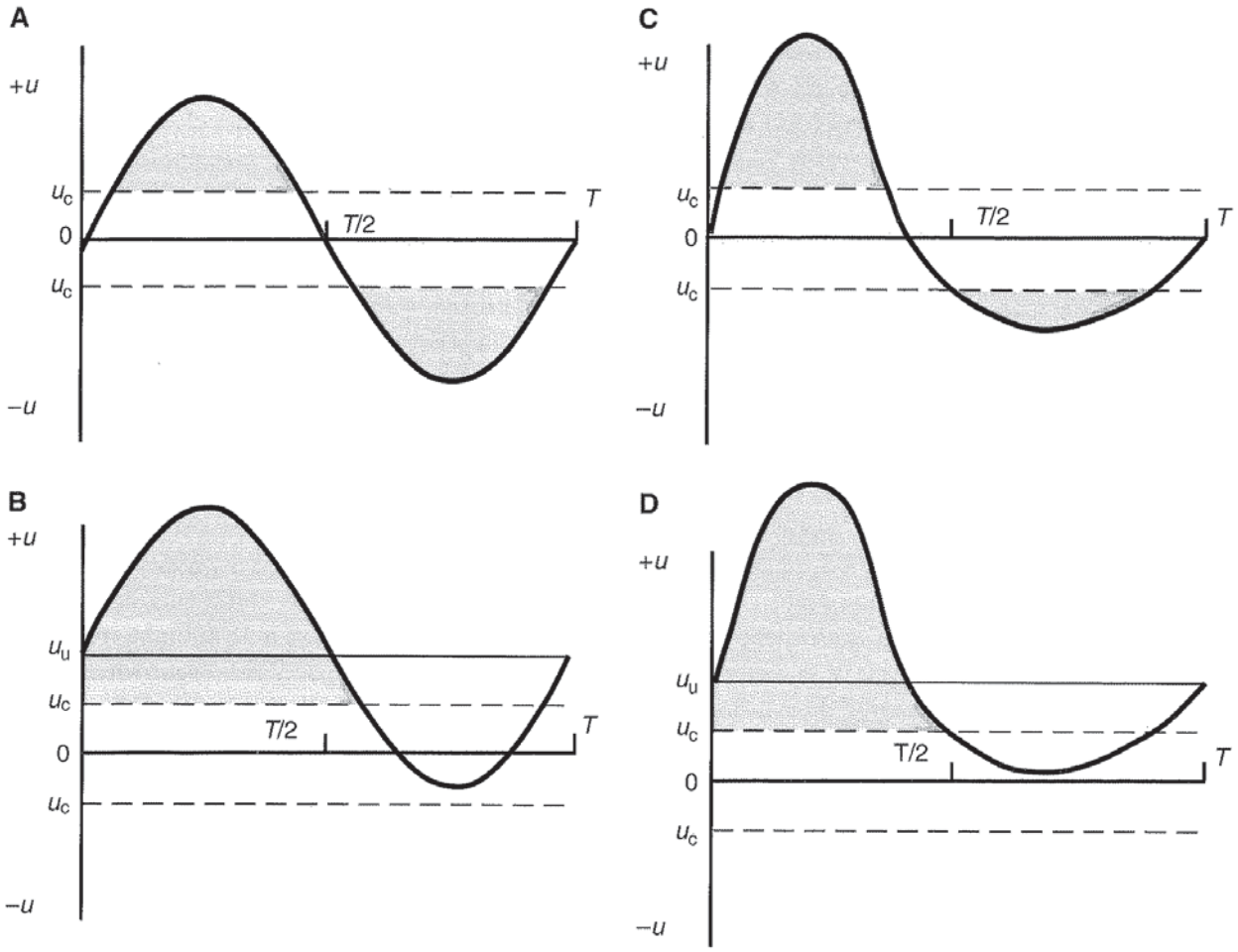

FIGURE 7.16. Hypothetical sediment transport by symmetrical and asymmetrical oscillatory wave currents and combined wave and unidirectional currents. (A) Variation over a wave period, T, of the horizontal component of the wave orbital velocity in the direction of wave motion, $+u$, and in the opposite direction, $-u$, for the case of a symmetrical, sinusoidal Airy wave. The threshold of sediment transport, u_c, is indicated, and the shaded areas represent periods when sediment transport occurs. (B) As for (A), but with a steady unidirectional current, u_u, added to the wave motion. (C) Orbital velocity variation and sediment transport for an asymmetrical Stokes wave. (D) As for (C), but with a steady unidirectional current, u_u, added to the wave motion.

increases, as is the case for bed sediment under unidirectional water flows. This suggests a common sorting process, but more details of the suspension threshold are needed to evaluate this. Beach sands are traditionally considered to be well sorted, and this is partly due to the fact that they are commonly fine- to medium-grained sands, and such sands are always well sorted (Chapter 5). However, the good sorting of beach sands may also be due to the constant reworking of beach sands by waves and to deflation by wind, both of which remove the fine-grained fraction in suspension. Alongshore variation in the mean grain size of beach sediment is expected in view of alongshore variation in the velocity of longshore currents. Shape sorting may also occur. The heavier grains of a given density and mean size (spheres) are more difficult to move than the lighter grains (flat grains such as disks), and will therefore require stronger currents to move them.

Bed forms and sedimentary structures due to wind waves and associated currents

Ripples form on a bed of cohesionless sand beneath wind waves at relatively low near-bed orbital velocities above the threshold of grain motion (Figure 7.14A). At larger near-bed orbital velocities, plane beds occur. The transition from wave ripples to plane beds occurs at a dimensionless bed shear stress of about 0.6 (Figure 7.14A), which is similar to the value for transition to upper-stage plane beds under unidirectional water flows. Plane beds beneath wind waves are probably dynamically similar to upper-stage plane beds. These bed configurations are modified in combined (oscillatory and unidirectional) flows, and new types appear. The origin, geometry, and dynamics of bed forms under wind waves and associated currents are

described here, together with their associated sedimentary structures. These include ripples, hummocks and wave-modified dunes, and plane beds. Larger-scale bed forms are also associated with wind waves and associated currents, including longshore bars (ridge-and-runnel structures) and beach cusps at shorelines, and longitudinal ridges formed in shallow water. These larger-scale bed features are discussed in Chapter 15 on coasts and shallow seas.

Wave ripples

At the threshold of bed-grain movement, just above wave base, there is little asymmetry in near-bed orbital velocities. As sediment begins to move backwards and forwards on the bed, low ripples ($L/H > 10$) that are symmetrical in profile (so-called rolling-grain ripples) start to form (Figure 7.18). The length of rolling-grain ripples is less than the near-bed orbital diameter. At greater near-bed orbital velocities, ripples grow in height until flow separation occurs on alternate sides of the ripple (so-called vortex ripples: Bagnold (1946)). Vortex ripples have heights, H, of 0.003–0.25 m, lengths, L, of 0.009–2.5 m, and L/H ratios between 4 and 10 mainly (Allen, 1979a, 1982a, 1985) (Figures 7.17 and 7.18). The wave length of vortex ripples ranges from 0.65 to1.0 times d_{ob}, most commonly $0.8d_{ob}$, up to a limiting orbital diameter beyond which the ripple length remains approximately constant but increases with mean grain size: commonly around 0.04 m in very fine sand to 1 or 2 m for very coarse sand and gravel (Miller and Komar, 1980) (Figure 7.18A). The relationship between vortex ripple length and grain size exists because the near-bed orbital velocity (and bed shear stress) is proportional to the orbital diameter for a given wave period. Vortex ripples have a symmetrical trochoidal profile (in the absence of asymmetrical wave currents) and long, straight crestlines in plan, and thus are commonly referred to as two-dimensional (2D) wave ripples. Crestlines have characteristic bifurcations (Figure 7.17). Paleowave conditions have been interpreted from the geometry of vortex-wave ripples observed in ancient deposits (e.g., Komar, 1974; Allen, 1981; Clifton and Dingler, 1984; Diem, 1984).

At still larger near-bed orbital velocities, 2D vortex ripples change to 3D (dome-shaped; circular to elliptical in plan) wave ripples (Southard *et al.*, 1990) (Figure 7.17). Three-dimensional wave ripples formed under waves with large orbital diameters and periods may have heights of decimeters and lengths up to several meters, and such large bed forms have been called *hummocks*. There is some disagreement over whether hummocks are large 3D wave ripples or a kind of wave-modified dune formed under combined flows (see below). At near-bed orbital velocities close to the transition to plane beds, L/H of wave ripples increases markedly (Figure 7.18A), and they become *postvortex (anorbital) wave ripples.*

Wave ripples formed in shoaling water are asymmetrical in profile, with the steep side facing the direction of shoaling (Figure 7.17), as a result of the net drift of the near-bed fluid. Such asymmetrical ripples may look superficially like current ripples, and care must be taken to distinguish them (Reineck and Wunderlich, 1968a). Two key differences between asymmetrical wave ripples and current ripples are that wave ripples have a smaller L/H ratio and are straight-crested. The L/H ratio of current ripples is commonly around 20, and current ripples never have long straight crestlines. *Interfering wave ripples* (Figure 7.17) occur where more than one set of waves (usually two) with different orientations occur in an area. Each set of waves simultaneously forms a distinctly oriented set of wave-ripple crests. The different wave sets may be associated with incident and reflected waves at a coastline. Interfering wave ripples are particularly common on tidal flats, where there are many bars that can reflect and refract waves. On tidal flats, wave ripples may also form interfering patterns with tidal current ripples.

Wave ripples will also become asymmetrical in profile under a combination of wind-wave currents and unidirectional currents. Addition of only a modest unidirectional current (0.1 m s^{-1}) to oscillatory currents will result in a degree of bed-form asymmetry that is difficult to distinguish from that due to purely unidirectional currents (Myrow and Southard, 1991; Dumas *et al.*, 2005) (Figure 7.19). It is therefore expected that combined flows will produce bed forms that are difficult to distinguish from those formed under unidirectional currents.

The pattern of flow and sediment transport over symmetrical and asymmetrical vortex wave ripples is rather complicated (Figure 7.20). As the crest of the wave passes, a flow-separation zone containing a high concentration of suspended sediment forms on the side of the wave ripple facing the direction of wave motion. As the trough passes, the same thing occurs on the other side of the ripple. In the intervening periods, the separation vortices and suspended sediment rise above the ripple (Bagnold, 1946; Longuet-Higgins, 1981), and this is an important mechanism for dispersing suspended sediment up from the bed. The growth of

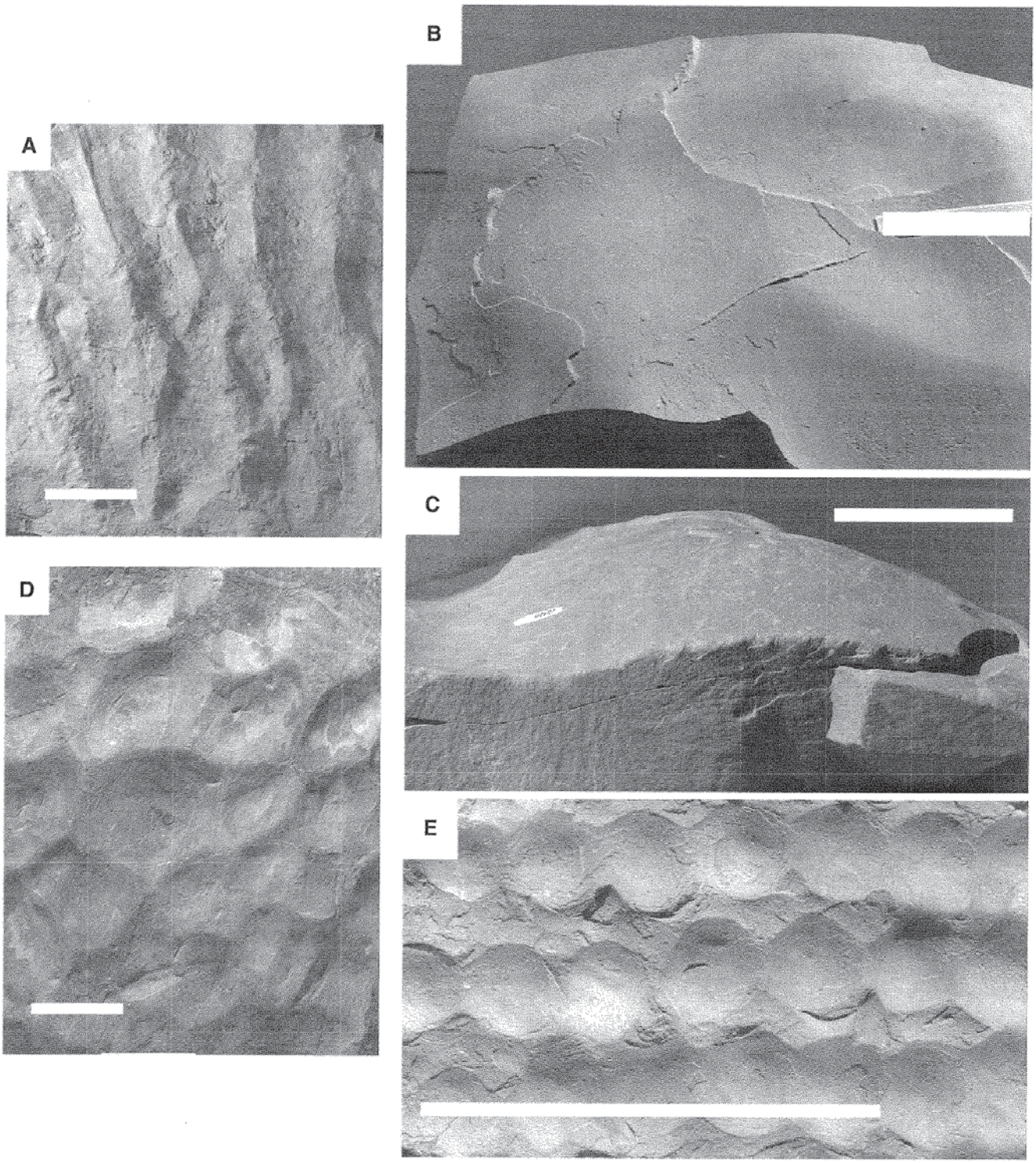

FIGURE 7.17. Ancient examples of (A) two-dimensional (2D) symmetrical vortex wave ripples, (B) and (C) three-dimensional hummocky wave ripples, and (D) and (E) interfering wave ripples. The white scale bars are 0.1 m long. Modern examples of (F) 2D symmetrical vortex wave ripples with a smaller set of wave ripples in troughs, (G) 2D asymmetrical vortex wave ripples with a set of superimposed symmetrical wave ripples, and (H) vortex wave ripples with double crests.

wave ripples is actually related to a non-periodic net drift of near-bed fluid and sediment from ripple troughs to crests, as confirmed in the visualization studies of Honji *et al.* (1980).

Symmetrical wave ripples generally do not migrate, because of the symmetry of the near-bed orbital velocities. However, natural wave currents are never completely symmetrical, and individual wave ripples may migrate for short distances either in the direction of wave motion or in the opposite direction. Since there is not expected to be any net sediment transport under symmetrical wave currents, erosion and deposition are

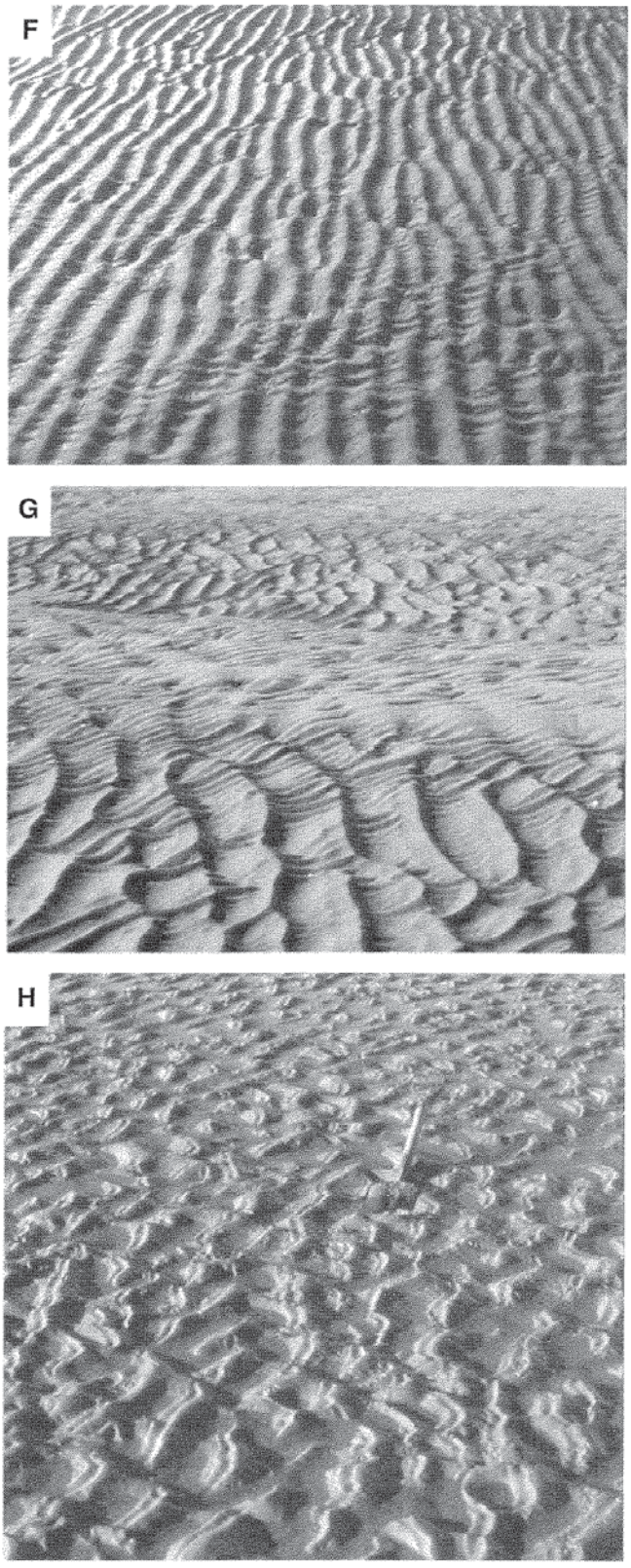

FIGURE 7.17. Continued.

not expected. Asymmetrical wave ripples migrate in the direction of the dominant current. Since there is net sediment transport in the case of asymmetrical wave currents and combined wave–unidirectional currents, there is the possibility of net erosion or deposition if the sediment-transport rate changes in the net transport direction.

Sedimentary structures formed by wave ripples and associated currents

Sediment laminae are draped on both sides of vortex wave ripples, including in their trough regions (Boersma, 1970; de Raaf *et al.*, 1977; Allen, 1982a) (Figure 7.21). Since symmetrical wave ripples can change their geometry and move short distances, different sets of inclined laminae can be produced and superimposed on each other (Figure 7.21). In views parallel to straight wave crests, the laminae appear almost horizontal, planar, and parallel. Slightly asymmetrical wave ripples also have laminae draped along both sides, but the laminae are preferentially developed on the steeper side that faces the direction of net sediment transport (Figure 7.21). As the degree of ripple asymmetry increases, sets of cross laminae form only on the steepest face, and these cross strata look similar to those formed by current ripples in views parallel to the flow direction (Figure 7.21). Cosets of such wave-ripple cross laminae can form because wave-ripple height changes during migration, and because deposition is possible with asymmetrical wave currents. Such asymmetrical wave-ripple laminae are commonly of the climbing type (Figure 7.21) when the deposition rate is high. Quantitative relationships among wave-ripple height, deposition rate, and cross-set thickness have not yet been developed. It is probable that cross laminae formed by combined flows would be almost indistinguishable from those formed by unidirectional currents.

Sediment laminae are also draped on 3D wave ripples as the ripples grow and migrate under depositional conditions. If the ripples were symmetrical, such cross laminae would appear the same in cross sections in any direction (Figure 7.22). If 3D wave ripples became asymmetrical they could migrate laterally, and net deposition would be possible. For high rates of deposition, cross laminae formed both on crests and on troughs of ripples can be preserved, forming what is known as *hummocky cross stratification* (HCS) (Figure 7.22). This is the 3D wave-ripple equivalent of climbing-ripple cross stratification (Chapter 5, Figure 5.60). For lower deposition rates, the laminae formed on the crests of the ripples cannot be preserved, and trough laminae are preferentially preserved, giving rise to *swaley cross stratification* (SCS). The terms hummocky and swaley cross stratification have tended to be

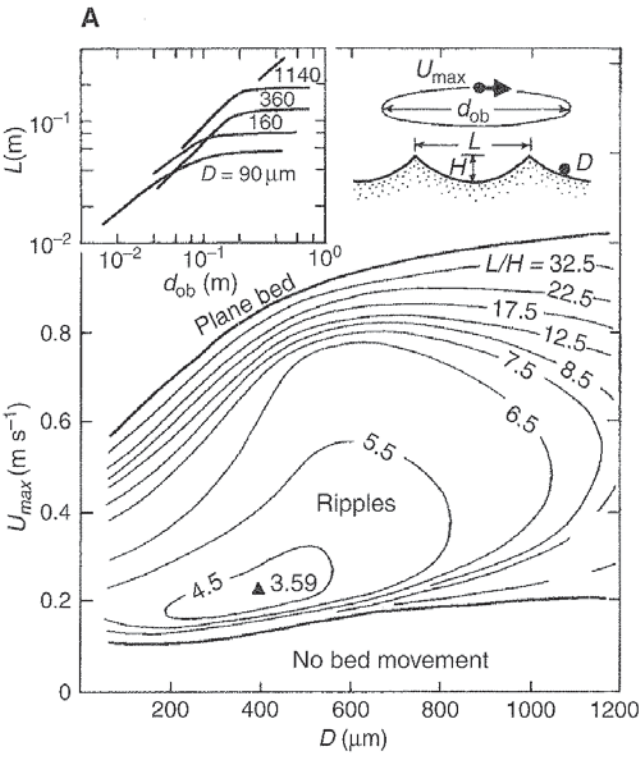

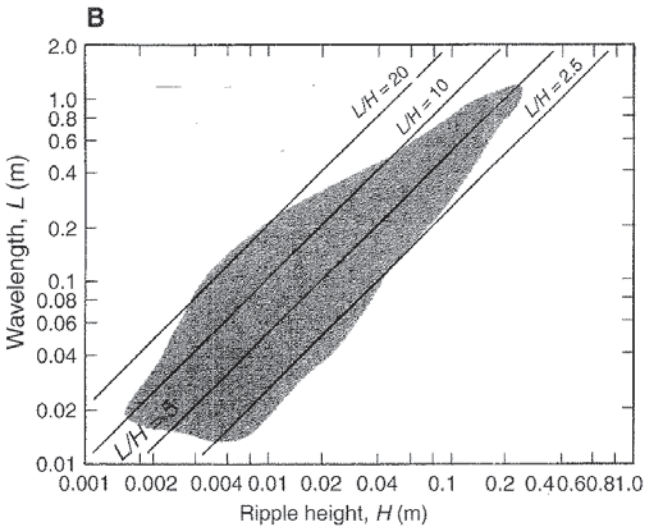

FIGURE 7.18. Geometry of wave ripples. (A) The length and height of laboratory wave ripples as functions of the maximum near-bed orbital velocity, mean grain diameter, and orbital diameter. From Allen (1985), based on Allen (1979a) and Miller and Komar (1980). (B) The length and height of wave ripples. From Leeder (1999), after Allen (1982a).

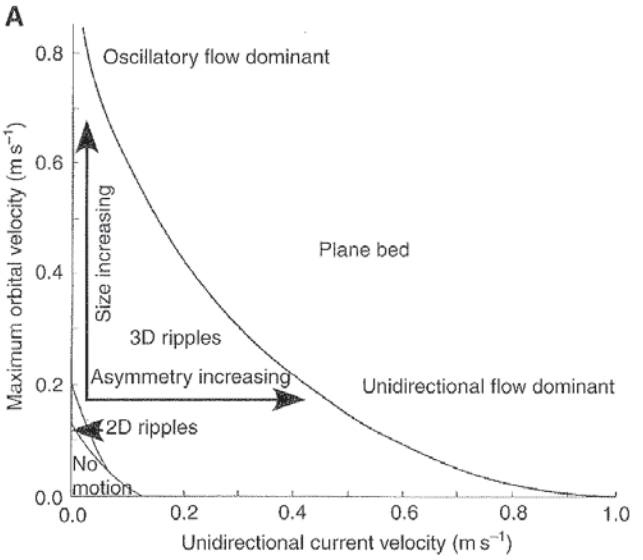

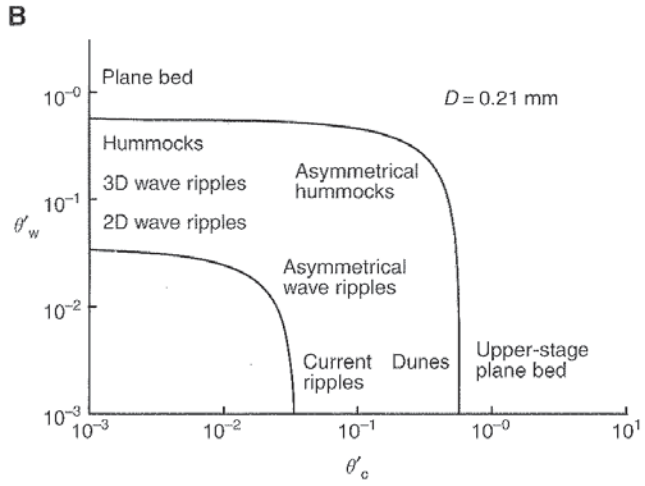

FIGURE 7.19. The equilibrium hydraulic stability of small-scale bed forms under combined wave currents and unidirectional currents, based on experimental data, in terms of (A) the water velocity, modified from Myrow and Southard (1991), and (B) the dimensionless bed-grain shear stress, courtesy of Maarten Kleinhans.

reserved for stratification associated with hummocks (and adjacent swales) that are meters across and decimeters high, with side slopes not exceeding 15°. However, cross strata formed by smaller 3D wave ripples are identical except for their scale (Craft and Bridge, 1987).

There has been much debate and disagreement about the origin of hummocky and swaley cross strata, because they have never been directly observed forming under natural conditions (e.g., Dott and Bourgeois, 1982; Harms *et al.*, 1982; Hunter and Clifton, 1982; Swift *et al.*, 1983; Walker, 1984; P. A. Allen, 1985;

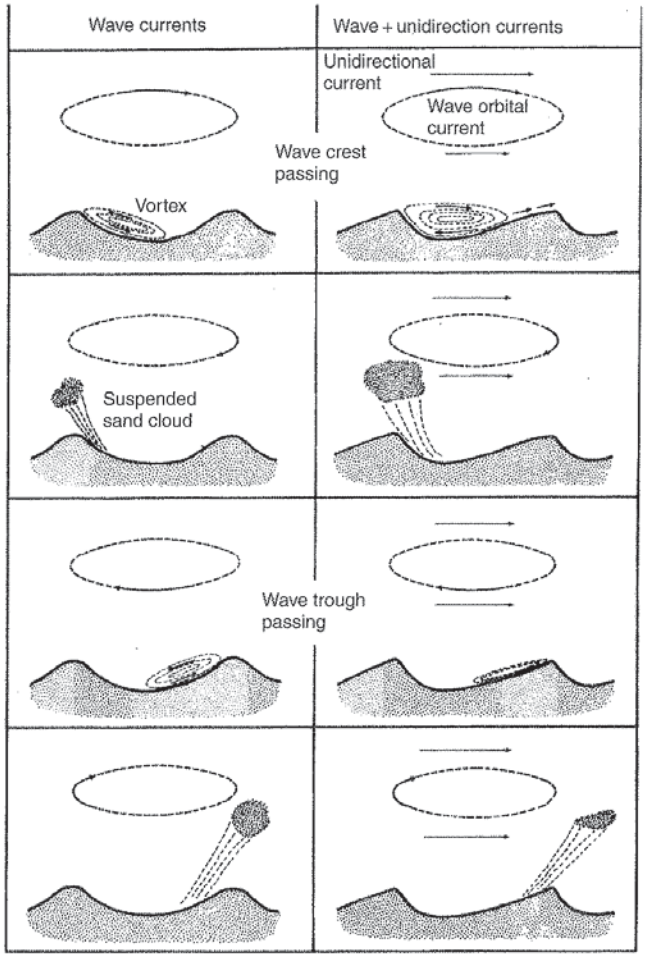

FIGURE 7.20. Flow and suspended-sediment transport over vortex wave ripples during a single wave period for the cases of wave currents only (left) and combined wave and unidirectional currents (right). Modified from Komar (1976).

Duke, 1985, 1990; Greenwood and Sherman, 1986; Leckie and Krystinik, 1989; Duke *et al.*, 1991; Amos *et al.*, 1996; Li and Amos, 1999). This is because HCS and SCS most likely form under very large waves during storms at sea when observation of bed conditions is difficult or impossible. Such conditions obviously cannot be reproduced in laboratory wave tanks, although Southard *et al.* (1990) and Dumas *et al.* (2005) have attempted to simulate waves with large orbital diameters and periods by using a flume in which the direction of unidirectional flow was periodically reversed. Hummocky bed forms have been observed on the sea bed following storms (e.g., Swift *et al.*, 1983), but it is not known what the bed configuration looked like during the storm, and there are insufficient observations of the internal structure of the bed. Several questions that have been debated are the following. (1) How is it possible for decimeter- to meter-thick cosets of HCS and SCS to form without appreciable deposition rate, and hence net sediment transport? (2) Why does the erosion surface at the base of cosets of HCS and SCS commonly show evidence of unidirectional currents, such as flute marks, gutter casts, and tool marks? (3) Do hummocks form only under combined flows? (4) What is the exact nature of the combined flows?

The erosion surface at the base of HCS and SCS units has been associated with offshore-directed unidirectional flows such as turbidity currents and geostrophic currents (e.g., Walker, 1984; Leckie and Krystinik, 1989; Duke, 1990). Ancient hummocky cross-stratified sandstone units typically pass laterally into thinner, finer-grained units composed mainly of wave-ripple cross lamination. This suggests that the magnitudes of bed shear stress and sediment-transport rate decrease in the direction of net sediment transport, which requires either asymmetrical wave currents and/or combined currents. The unidirectional currents that formed the basal erosion surface could also have deposited the overlying sediment that was molded into hummocks by strong wave currents. However, it is rare to find evidence for strong unidirectional currents in HCS and SCS, such as stratal dips (including angle-of-repose cross strata) directed preferentially in the direction of thinning and fining of the deposit. It is known also that a unidirectional current with a velocity of as little as $0.1\,\mathrm{m\ s^{-1}}$ can cause wave ripples to become markedly asymmetrical. Therefore, HCS and SCS are probably formed by strong oscillatory wave currents, with only a minor unidirectional current superimposed (P. A. Allen, 1985; Nottvedt and Kreisa, 1987; Arnott and Southard, 1990; Myrow and Southard, 1991; Dumas *et al.*, 2005). Hummocks are therefore not wave-modified dunes. As the magnitude of the unidirectional current increases relative to the magnitude of the oscillatory current, the hummocky bed form will become markedly asymmetrical and angle-of-repose cross strata will form. Such a combined flow would have a larger absolute magnitude, resulting in coarser-grained sediment (e.g., Nottvedt and Kreisa, 1987; Arnott and Southard, 1990; Cheel and Leckie, 1992; Bridge and Willis, 1994).

If HCS units are formed during storms that last on the order of days, a unit on the order of decimeters thick would require deposition rates on the order of $10^{-3}\,\mathrm{mm\ s^{-1}}$. Since the near-bed sediment concentration is very high during major storms at sea, a small change in a large sediment-transport rate with distance could yield such deposition rates. However, there has been no quantitative work on the relationship among hummock height, deposition rate, and set thickness.

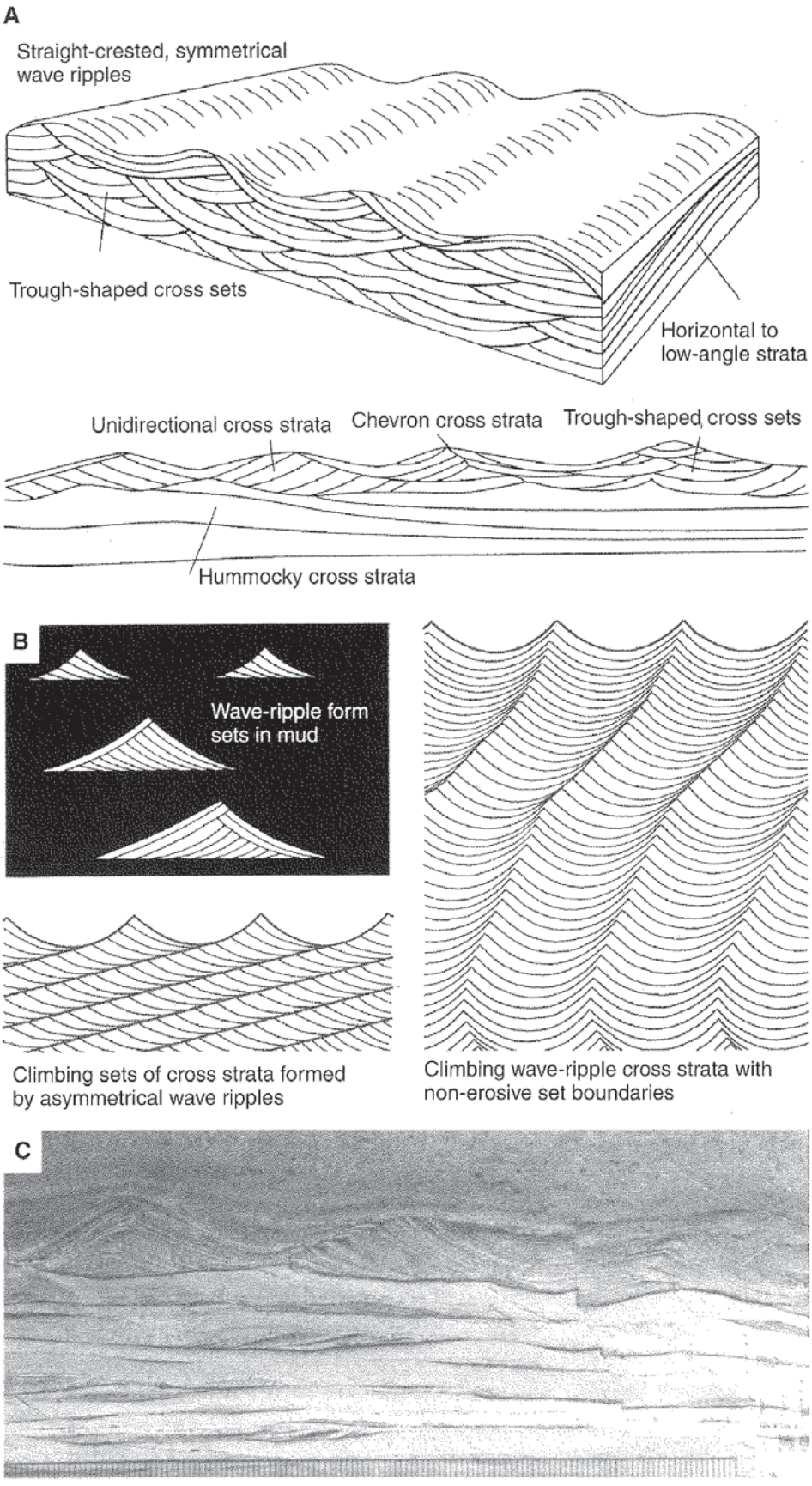

FIGURE 7.21. Types of cross strata formed by wave ripples. (A) Modified from Boersma (1970). (B) Modified from Allen (1982a). (C) A field example of cross strata formed by symmetrical and asymmetrical wave ripples (scale in millimeters).

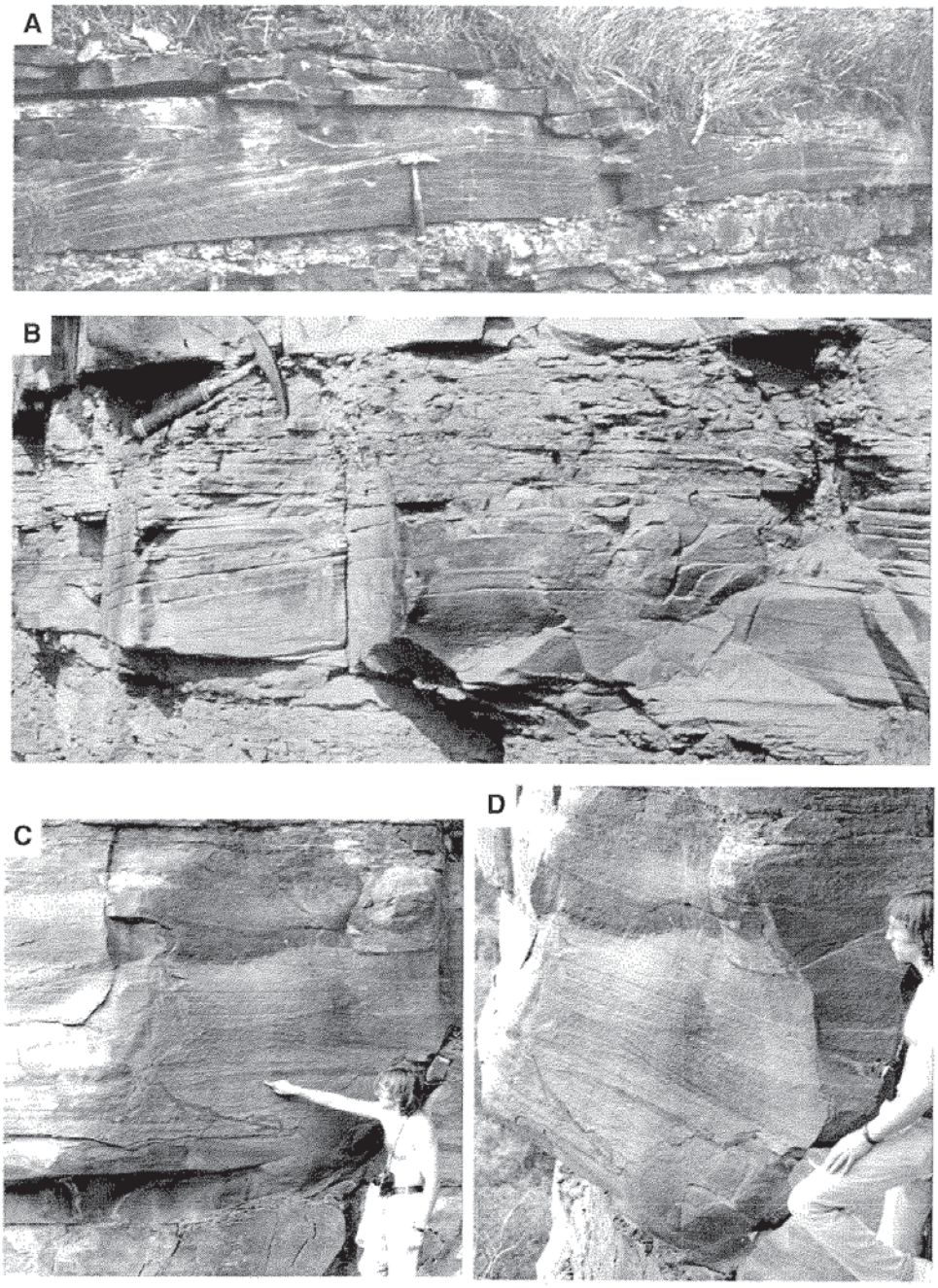

FIGURE 7.22. Hummocky cross strata, (A) and (B), and swaley cross strata in orthogonal views, (C) and (D).

Plane beds and planar lamination

Plane beds form beneath waves with large near-bed orbital velocities, and in the surf zone of sandy beaches (Figure 7.23). Although these plane beds appear to be dynamically similar to the upper-stage plane beds of unidirectional turbulent flows, there are obviously some differences. Water flow reverses periodically under waves, and, as far as we know, low-relief bed forms have not been observed on wave-formed plane beds.

Deposition on wave-formed plane beds forms planar lamination that looks remarkably like that developed on upper-stage plane beds. However, it cannot have formed the same way. The individual laminae are most likely formed by the periodic deposition associated with the reversing wave currents as individual waves pass. However, if strong unidirectional currents are superimposed on wave currents, it is uncertain which current is responsible for the planar laminae. In the surf zone of sandy beaches, the planar laminae have characteristic concentrations of heavy minerals (Figure 7.23). This is the well-known *beach lamination* (Clifton, 1969; Reineck and Singh, 1980; Allen, 1982a). The character of sets of these laminae can be influenced

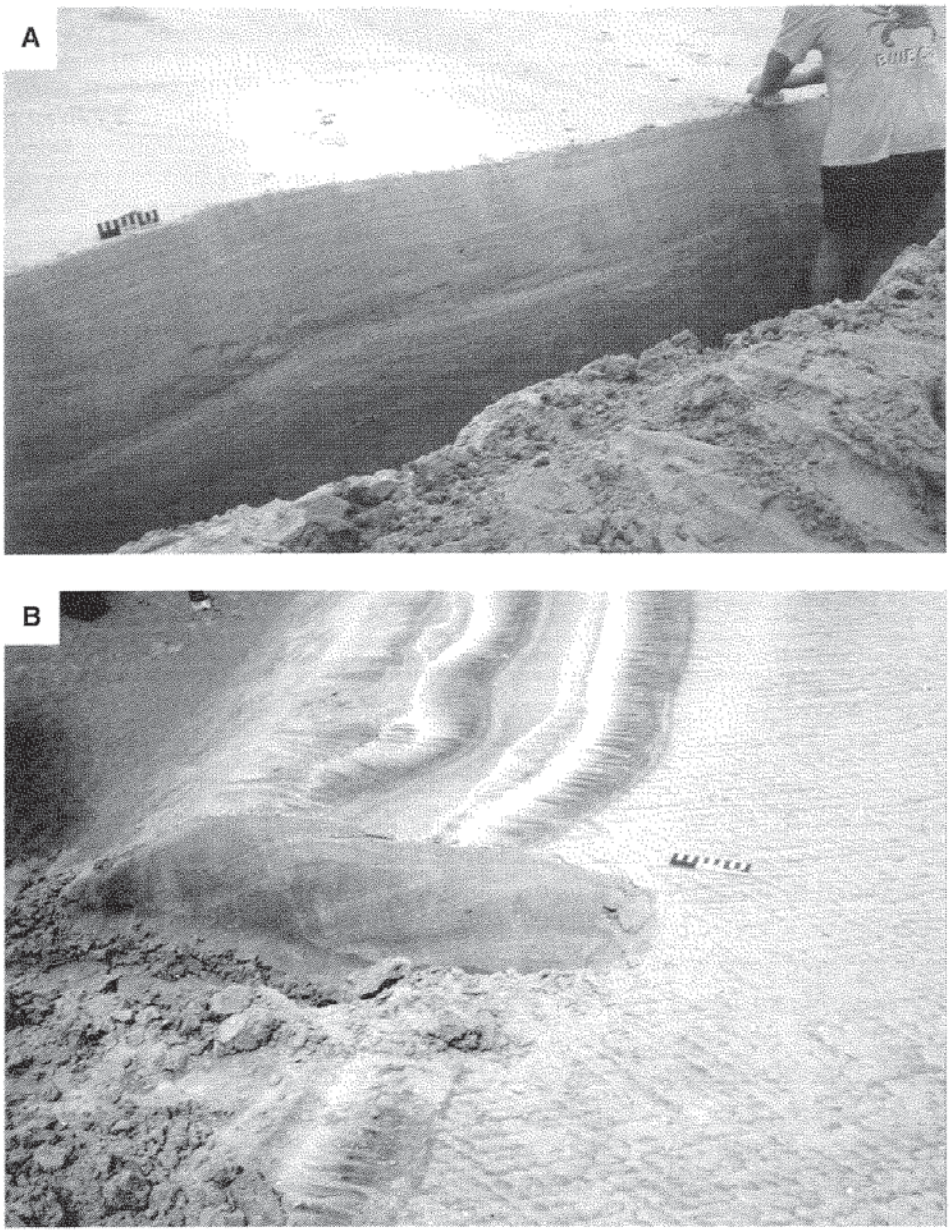

FIGURE 7.23. (A) A wave-formed plane bed on a beach and associated planar laminae. (B) The crest area of a longshore bar on a beach, showing rhomboid ripple marks, antidunes, and inclined strata associated with onshore migration of the steep lee face.

by tides, storms, or storm seasons. It is unknown whether low-relief bed forms play any role in the formation of laminae by wave currents.

Hydraulic criteria for the existence of equilibrium bed states under wind waves

The equilibrium hydraulic stability fields of bed states formed by purely oscillatory wave currents can be expressed in terms of the dimensionless bed shear stress and grain Reynolds number, as is the case for unidirectional water flows (e.g., Komar and Miller, 1975b; Miller and Komar, 1980) (Figure 7.14A). Simpler stability diagrams have been constructed using u_{max} and the mean grain size (Allen, 1979a, 1982a, 1985), see Figure 7.18A, and u_{max}, mean grain size, and wave period (Harms *et al.*, 1982). However, these diagrams are based mainly on experimental data. More data from natural environments are needed, especially relating to larger-scale bed forms such as hummocks. There is also a pressing need for equivalent diagrams for a wide range of types and orientations of combined flows. Myrow and Southard's (1991) diagram (Figure 7.19) was a good start, but it is not general enough. However, Kleinhans (personal communication) has used a broad range of laboratory and field data to define the hydraulic stability fields of combined-flow bed forms in terms of dimensionless bed shear stress (Figure 7.19). Hydraulic stability diagrams can be used to predict sequences of bed forms

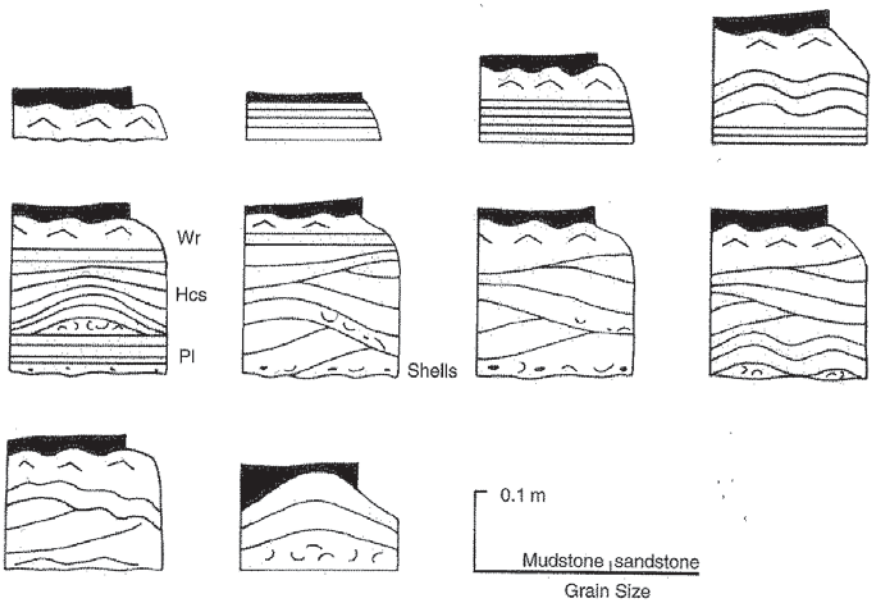

FIGURE 7.24. Typical vertical sequences of grain size and sedimentary structures due to waves. After Craft and Bridge (1987). Black is mudstone; white is sandstone. Bases of stratasets are sharp and erosional, and may contain flute marks, gutter casts, tool marks, and burrows. Burrows also occur in upper parts of stratasets. Top parts of stratasets may be eroded. Wr = wave-ripple lamination, Hcs = hummocky cross strata, Pl = planar strata.

and sedimentary structures formed under changing hydraulic conditions (e.g., Allen, 1985; Myrow and Southard, 1991) (Figure 7.24).

Generation of tides

Tides in the world's oceans are produced by the gravitational attraction between the Earth, Moon, and Sun. The tide-generating force is actually the resultant of the gravity force and the centrifugal force arising from co-rotation of the Earth, Moon, and Sun. The manifestation of the tide-generating force is deformation of the water surface of the Earth into an oblate spheroid, producing bulges in the water surface and concomitant hydrostatic pressure gradients. The so-called *equilibrium tide* is that where the hydrostatic pressures and tide-generating forces are balanced. The Moon has the dominant effect on ocean tides, and the Sun's effect is about half as strong because of its greater distance from the Earth. Figure 7.25A shows the Earth with bulges in the surface of the ocean (equivalent to high tides) on opposite sides of the Earth, caused mainly by the gravitational attraction of the Moon. The distance between the crests of these bulges (and the length of a tidal wave) is half of the local circumference of the Earth. Since the Earth rotates on its axis once every 24 hours, an observer on the surface of the Earth will experience two high tides and two low tides every 24 hours approximately (semidiurnal tides). However, the Moon moves around the Earth every month, so semidiurnal tides have a period of 12.5 hours rather than 12 hours. This is why the time of high tide is later by about one hour every day. The tidal wave amplitude actually differs for successive semidiurnal tides (the *diurnal inequality*) because of the declination of the Earth's rotational axis (Figure 7.25B). As the Moon moves around the Earth, the gravitational attractions of the Sun and Moon will vary in direction throughout the month. When the Earth, Moon, and Sun are all in line (full and new moons), the amplitude of the tidal bulges is at its maximum, producing the highest tidal range (*spring tides*, occurring twice per month). When the Moon and Sun form a right angle with the Earth (Figure 7.25C), their gravitational attractions act against each other, and the tidal bulges have their minimum amplitude and tidal range (*neap tides*). This is a simple picture of tidal periods and amplitudes. There are many more tidal periods and amplitudes related to factors such as the elliptical orbits of the Earth and Moon, and changes in the declination of the rotational axes of the Earth and Moon through their orbits (Table 7.2). Figure 7.25C explains seasonal changes in the amplitudes of neap tides and spring tides, and inequalities of successive neap and spring tides.

Tides on a perfectly spherical Earth, with no friction between the water and the Earth, would have a maximum tidal range of less than 1 m. However, tidal ranges near coastal areas can be much greater than this, and may reach more than 15 m. Tidal waves in the open ocean are amplified as they approach land masses, due to the effects of (1) flow convergence, (2) wave reflection, and (3) Coriolis deflection. Tidal range may also be damped by friction between the water and the Earth's surface. The effects of these tide-modifying factors on tidal ranges and currents are discussed below.

TABLE 7.2. Most important tide-generating constituents (from Defant, 1958)

Type of tide	Symbol	Period (solar hours)	Relative amplitude	Constituent
Semidiurnal	M_2	12.42	100.00	Main lunar
	S_2	12.00	46.6	Main solar
	N_2	12.66	19.1	Monthly variation in Moon's distance from Earth
	K_2	11.97	12.7	Changes in declination of the Sun and Moon during orbits
Diurnal	K_1	23.93	58.4	Solar–lunar
	O_1	25.82	41.5	Main lunar
	P_1	24.07	19.3	Main solar
Long period	M_f	327.86	17.2	Moon's fortnightly

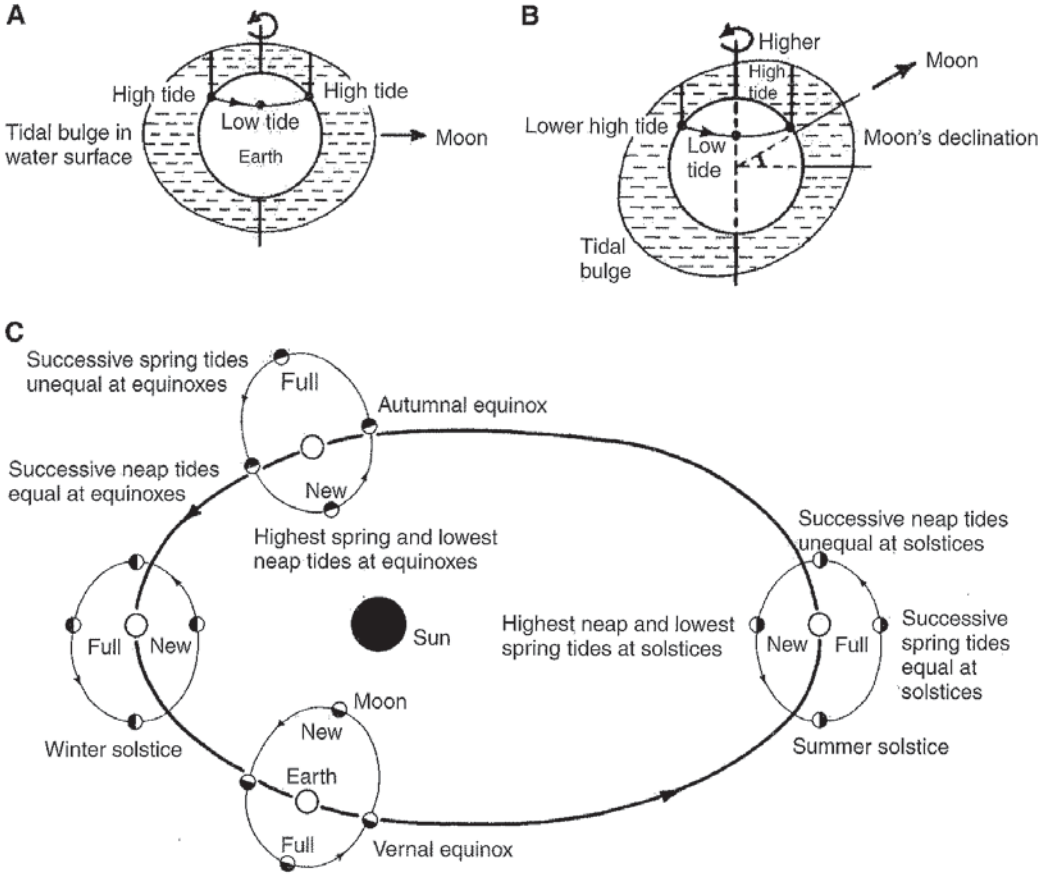

FIGURE 7.25. The origin of tides. (A) The bulge in Earth's ocean-water surface due to the position of the Moon explains the semidiurnal tidal period (two high tides and two low tides per day). (B) Diurnal inequality of semidiurnal tidal amplitudes due to Moon's declination. (C) The eccentric elliptical orbit of the Moon around Earth results in neap and spring tides (two of each per month), and inequality of successive neap-tidal amplitudes (at solstices) and spring-tidal amplitudes (at equinoxes). The eccentric elliptical orbit of Earth around the Sun results in changes in peak spring- and neap-tidal amplitudes. Modified from J. R. L. Allen (1985).

Tidal currents

Tidal waves are shallow-water waves ($L/d > 20$), and undergo a transformation similar to that undergone by wind waves as they move into shoaling water: the waves become asymmetrical in profile and their height increases. A breaking tidal wave is called a *tidal bore*. With asymmetrical tidal waves, water currents associated with the flood tide are stronger and of shorter duration than those associated with the ebb

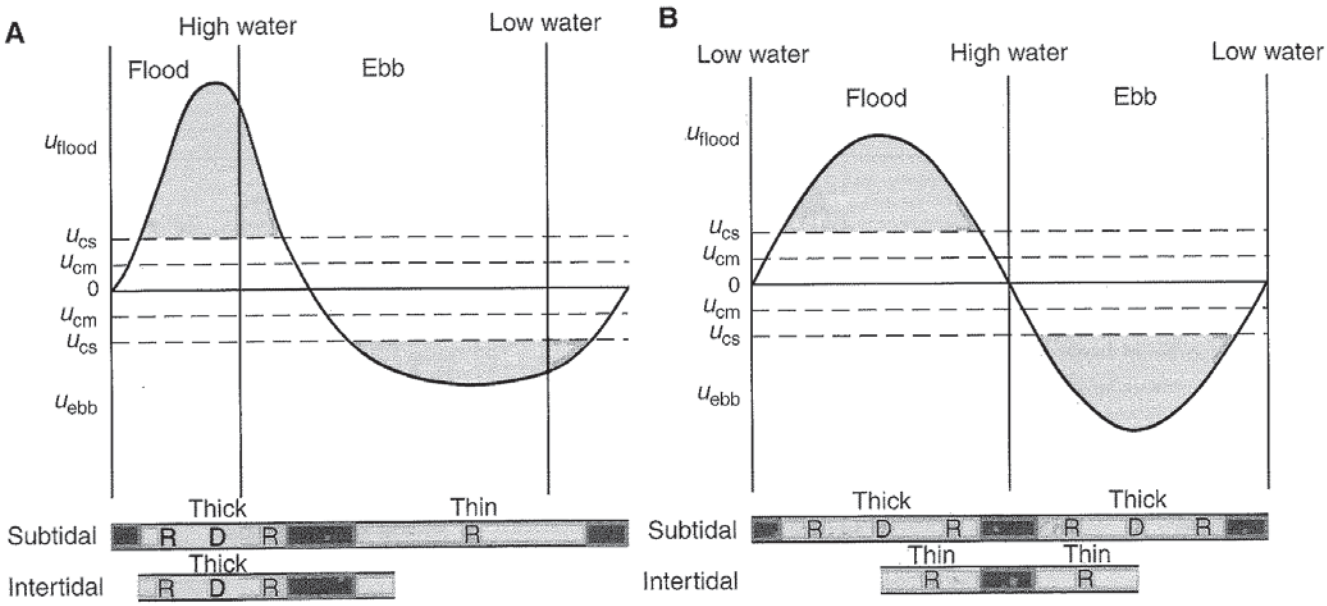

FIGURE 7.26. Idealized variation of tidal current velocity, u_{flood} and u_{ebb}, and sediment transport over one wave period for (A) an asymmetrical progressive tidal wave and (B) a symmetrical, standing tidal wave. Thresholds of sediment motion for sand, u_{cs}, and mud, u_{cm}, are indicated, and the light-shaded areas are periods of sand motion. Under the assumption that deposition occurs throughout the tidal cycle, and that peak tidal currents are strong enough to form dunes, the relative thickness, grain size, and internal structure of the deposits in subtidal and intertidal locations are suggested. Dark shading indicates mud, and light shading indicates sand; R indicates ripple migration and associated small-scale cross strata; D indicates dune migration and associated medium-scale cross strata.

tide. The maximum flood currents occur close to the time of high tide, and the maximum ebb currents occur near the time of low tide (Figure 7.26). This means that topographically high coastal regions (e.g., upper tidal flats) will experience maximum flood-current velocities, and topographically low coastal areas (e.g., channels) will experience maximum ebb-current velocities. The maximum flood and ebb currents may well follow different paths at the coast, and inequality of durations and magnitudes of flood and ebb currents at a point is to be expected. The transformation of a tidal wave as it moves into shoaling water is associated with flow convergence in the vertical plane. However, tidal waves also converge in the horizontal plane as they move through straits between land masses, and as they move up estuaries. This convergence also increases tidal ranges (see Figure 7.27).

A tidal wave moving into an enclosed basin or estuary will be reflected at its end, and the reflected wave may interact with the next incoming tidal wave to give *resonant amplification*. When two waves of equal period and height travel in opposite directions, a standing wave with double the amplitude of the individual waves develops (see above). Resonant amplification of standing waves occurs when the length of the basin or estuary is 1/4, 3/4, 5/4, and so on, of the length of the standing wave, which is $T\sqrt{(gd)}$. The maximum tidal currents in standing waves occur at times of mid-tide level (Figure 7.26). However, it is likely that a tidal wave moving into an enclosed basin or estuary will also be modified by the effects of flow convergence, the Coriolis force, and bed friction. Therefore, a simple standing wave is unlikely, and the maximum tidal currents will not be associated with the mid-tide position. The Bay of Fundy in Newfoundland has the highest tide range in the world (spring tidal range >15 m), due to the effects of resonant amplification, flow convergence, and the Coriolis force. A quarter wave length of the standing wave with period 12.42 hours and mean depth 70 m is 290 km, which is very close to the length of the Bay of Fundy.

The Coriolis force deflects moving water to the right of its path in the northern hemisphere and to the left in the southern hemisphere. If a tidal wave in the northern hemisphere moves into an enclosed basin (e.g., the North Sea), a northward flow would be deflected towards the east side of the basin, and a southward flow would be deflected towards the west side of the basin. This flow deflection results in an amplification of tidal range that reaches a maximum at the coast, and a point in the center of the basin where the tidal range is zero (an *amphidromic point*). Another result is that the tidal wave moves around the basin in an anticlockwise

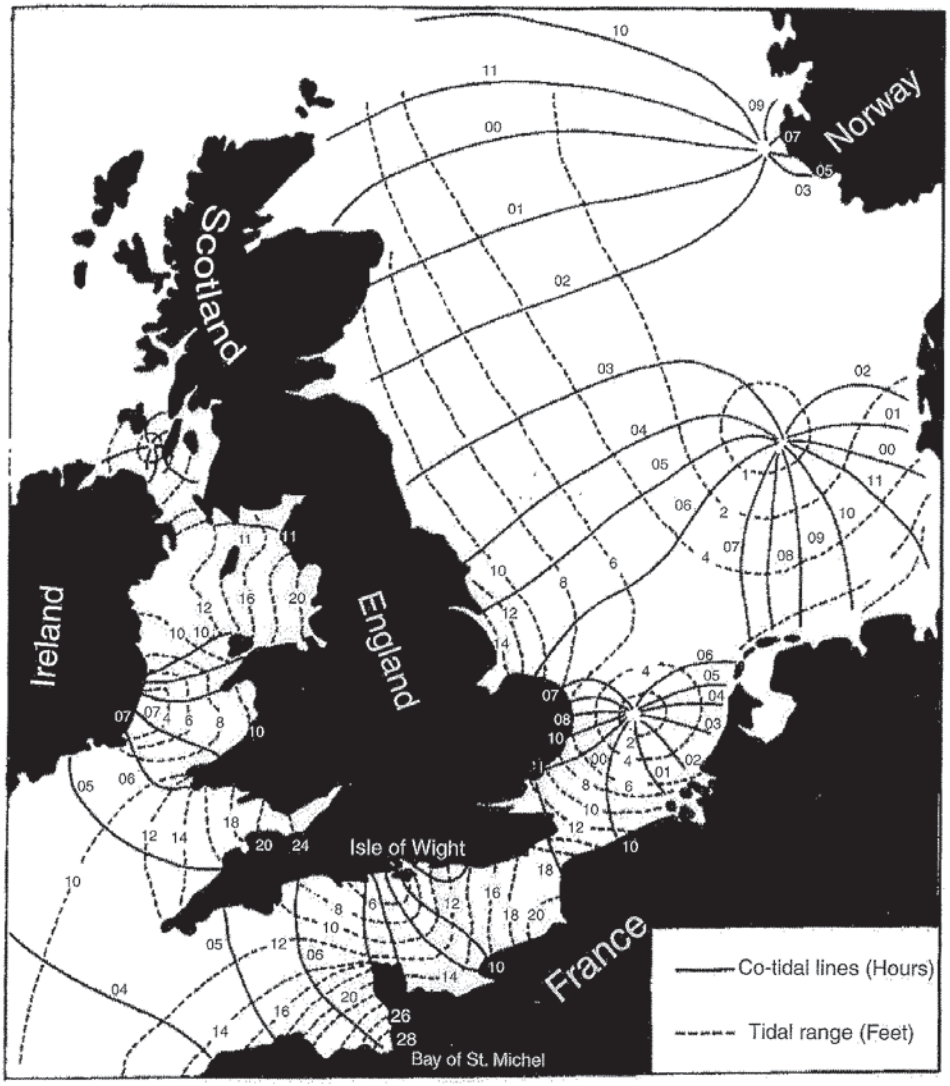

FIGURE 7.27. Tides around England. Co-tidal lines are positions of the tidal wave crest (high tide) throughout the daily cycle. In places, co-tidal lines indicate anticlockwise rotation of the tidal wave crest around amphidromic points, where the tidal range is zero. The tidal range (marked by dashed lines) increases away from amphidromic points and towards coastlines. The tidal range also increases into embayments and estuaries (e.g., the Severn), and towards the Straits of Dover, due to convergence of the tidal wave. From Komar (1998).

direction about an axis that is the amphidromic point (Figure 7.27). This means that tidal current directions vary around the basin rather than oscillating in a straight line parallel to a constant direction of tidal wave propagation. At a given point, the paths of water particles follow an elliptical path rather than oscillation about a line. In reality, tidal ellipses are not closed, are irregular in shape, and vary with depth at a point. Also, tidal currents in the North Sea are affected by flow convergence and wave reflection.

Bed friction causes damping of tidal waves, meaning reduction in wave height in the direction of wave propagation. Such damping modifies the nature of reflected tidal waves, because the reflected wave will be more damped than the incoming wave. Reduction in wave height in the direction of wave propagation can also result in the displacement of amphidromic points to one side of an enclosed sea or gulf (P. A. Allen, 1997).

Maximum tidal current velocities increase with tidal range and with shoaling, as is the case for all shallow-water waves (Equation (7.11)). In the case of a simple shallow-water wave with a height (tidal range) of 2 m in water 10 m deep, the maximum near-bed velocity would be about $1\,m\,s^{-1}$ using Equation (7.11). However, Equation (7.11) is not strictly applicable when flow is accelerated through channels or damped by friction over broad tidal flats. Nevertheless, it is common for maximum velocities of tidal currents to reach 1 or 2 meters per second in shallow enclosed seas and tidal channels. Tidal range (and associated current velocity) is commonly classified as *microtidal* (0–2 m),

mesotidal (2–4 m), and *macrotidal* (>4 m). These terms are used to indicate the relative importance of tidal currents in shaping coastal environments (see Chapter 15). Wind-wave currents are also important in shallow marine and coastal areas, and it is normal for superposition of tidal currents and wind-wave currents to occur.

Sediment transport by tidal currents

Tidal currents commonly have sufficient velocity to move sand and gravel on the bed, and silt and clay in suspension. The asymmetry of tidal currents in shallow water, and the fact that maximum flood and ebb currents commonly follow different paths, result in characteristic sediment-transport paths for which there is net sediment transport in a given direction (Figure 7.28) (Allen, 1970; Johnson *et al.*, 1982; Harris *et al.*, 1995). If the tidal range and maximum current velocity decrease in the direction of the sediment-transport path, the mean grain size of the sediment transported will decrease and deposition will occur. If the current velocity increases in the direction of net sediment transport, the mean grain size of transported sediment will increase and erosion will occur.

Since the maximum flood currents can affect topographically high areas, sediment can be deposited in these areas if the current velocity decreases in the direction of sediment transport. Such deposited sediment might not be removed by erosion by the weaker ebb currents. This is one reason for the preferential deposition of suspended mud in upper intertidal flats. Another reason may be that mud requires a greater bed shear stress to erode it than to deposit it. Deposition from a tidal current that is decelerating in time as well as space will give rise to a fining-upward

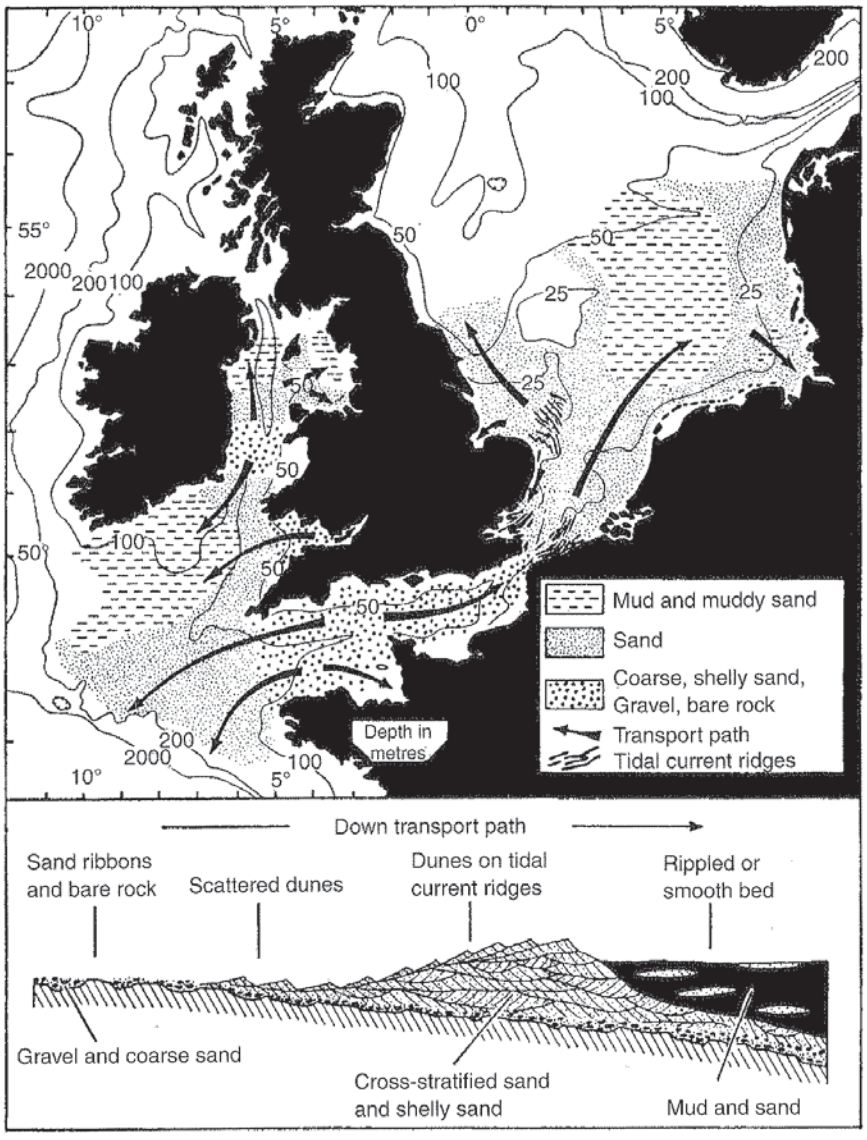

FIGURE 7.28. Sediment-transport paths associated with tidal currents around the North Sea. From Allen (1970).

unit, and deposition from a tidal current that is decelerating in space but accelerating in time will yield a coarsening-upward unit. If the deposition rate is on the order of millimeters per tidal cycle, a lamina could be formed during the flood tide, and another might be formed on the ebb tide (especially in areas below the low tide level). Such laminated deposits are called *laminites* (Figure 7.29A, B). The thickness of each lamina will be related to the deposition rate, the time over which it formed, and any subsequent erosion.

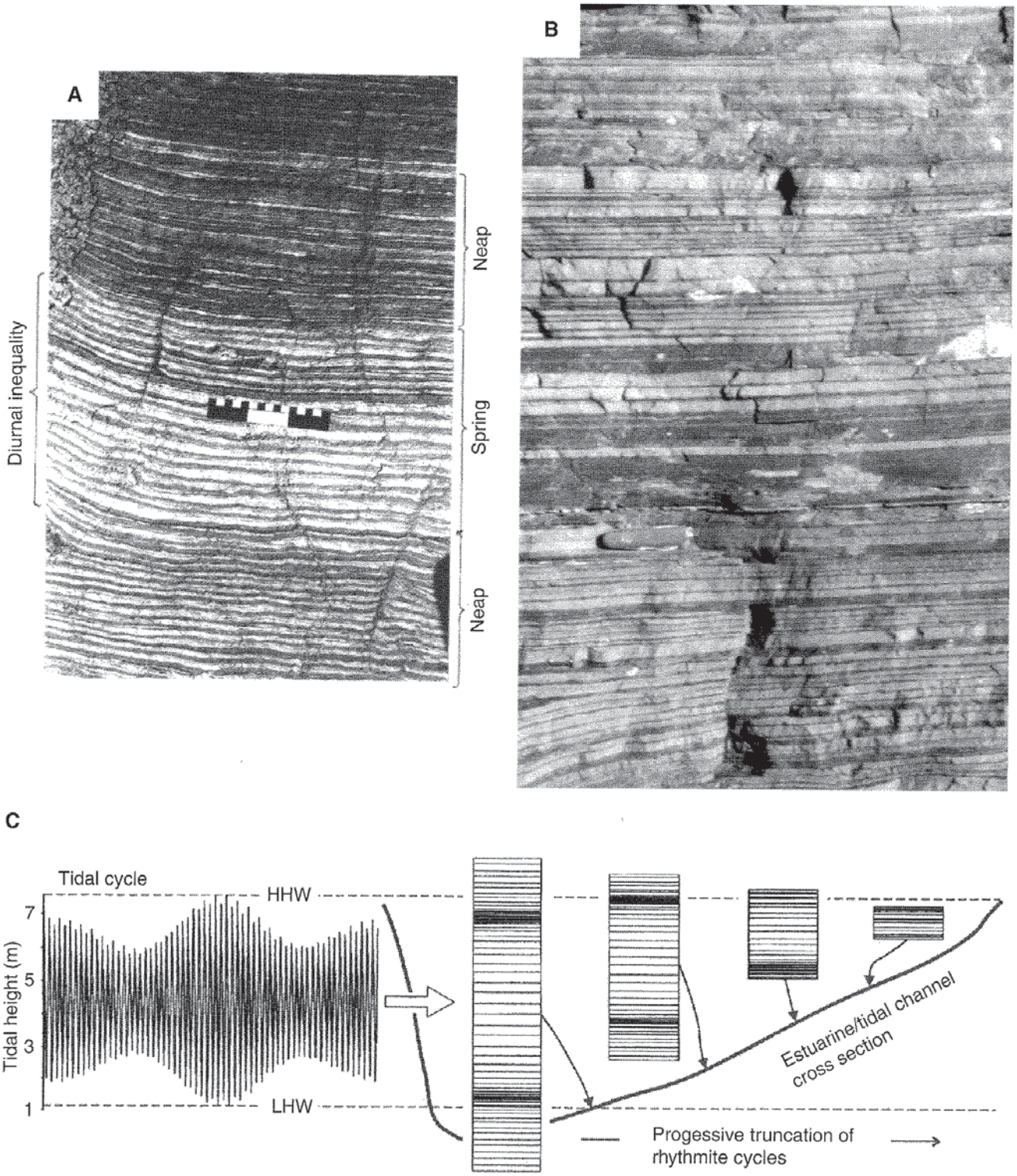

FIGURE 7.29. Tidal laminites. (A) Sandstone–shale couplets with variable sandstone/shale ratio, attributed to deposition over spring and neap tides. From Nio and Yang (1991). (B) Possible tidal laminites in limestones. (C) Decreasing preservation of tidal rhythmites as a function of elevation on a tidal flat. From Archer (1998).

Systematic variations in the thickness of laminae have been related to periodic variations in current strength and deposition rate over, say, spring–neap tidal cycles; see reviews by Nio and Yang (1991) and Archer (1998) and various papers in Smith *et al.* (1991) and Alexander *et al.* (1998). However, it is unlikely that thickness variations would follow periodicity in tidal range very closely in view of the effects of simultaneous non-periodic variation in wind-wave currents. Also, the relationship among tidal range, current velocity, and deposition rate might not be simple. Laminites formed in high intertidal regions may receive deposits only during the highest tides or major storms (Figure 7.29C). However, if 28 successive laminae exhibit a systematic thickening and thinning, it is difficult to avoid the interpretation of their having been formed during continuous deposition by semidiurnal tides over a spring–neap cycle.

Bed forms and sedimentary structures formed by tidal currents

Ripples and dunes are readily formed by tidal currents because the velocities required exist for on the order of hours (Figure 7.30). However, it is unlikely that the geometry of the larger bed forms is ever in equilibrium with the changing flow conditions. The common asymmetry of tidal currents means that different bed forms may exist in an area under flood and ebb conditions. Dunes commonly migrate in one dominant direction, although they may be modified by the flow in the opposite direction. Most tidal bed forms are influenced by simultaneous wave currents and by the effects of rising and falling water level. Larger-scale bed forms associated with tidal currents (on which ripples and dunes are superimposed) are tidal-current ridges, sand waves, and ebb- and flood-tidal deltas. These bed forms are discussed in Chapter 15 on coastal and shallow marine depositional environments.

Ripples

Ripples formed by tidal currents alone are essentially the same as those formed by unidirectional currents. However, tide-formed ripples are very commonly modified by wind-wave currents, and by the effects of falling water levels and reversing currents (Figure 7.30). Superposition of different patterns of tidal current ripples and wave ripples is common. As water flows off a rippled bed area during an ebbing tide, the crests of the ripples may be planed off. At any given time, the small-scale cross strata within a ripple may indicate flow in a direction different from that indicated by the ripple form. Superimposed sets of small-scale cross strata formed by tidal ripples (Figure 7.31) may indicate the occurrence of reversing flows if tidal currents were symmetrical (*herringbone cross stratification*). Such sets may also indicate flow in one direction if the tidal currents are strongly asymmetrical or if deposition from either asymmetrical or symmetrical tidal currents occurred only during the flood or ebb (in which case the formative flow could be misinterpreted as unidirectional).

In areas where ripples are formed by the maximum tidal currents, the ripples stop moving during the periods of slackening water flow (e.g., Figure 7.30). These ripples may then be draped with mud deposited from suspension. This mud is commonly pelleted by benthic invertebrates. If net deposition is proceeding, the alternations of rippled and cross-stratified sand and mud drapes formed during tidal cycles give rise to *heterolithic bedding* (Figure 7.31). Differences among varieties of heterolithic bedding depend on (1) the relative amounts of sand and mud in the deposits, depending on the current velocity and sediment supply during deposition; (2) the relative importance of tidal and wave currents during deposition; (3) whether the tidal currents are symmetrical or asymmetrical; (4) whether deposition occurs throughout the tidal cycle; and (5) whether the site of deposition was intertidal or subtidal.

Flaser bedding (Reineck and Wunderlich, 1968b; Reineck and Singh, 1980) occurs when mud drapes occur only in ripple troughs (Figure 7.31). *Wavy bedding* occurs when mud drapes over the whole of a continuous bed of rippled and cross-stratified sand. *Lenticular bedding* refers to isolated sand-ripple forms encased in mud. These types of heterolithic bedding are commonly associated with deposition on tidal flats. However, the basic alternation of sand and mud can occur in any environment where there is periodic variation in current strength. Specific features must be present for a tidal origin to be invoked, as explained below. In tidal settings, it is normally assumed that each mud drape in flaser and wavy bedding could be deposited during a single tidal cycle. However, the thicker mud layers in wavy and lenticular bedding could not be deposited during a single tidal cycle: there is not enough time given the expected suspended-sediment concentrations (McCave, 1970; Hawley, 1981). Such mud layers may be related to a sequence of tidal cycles or post-storm conditions. Mud layers should be examined closely to determine whether they are composed of sand-sized mud

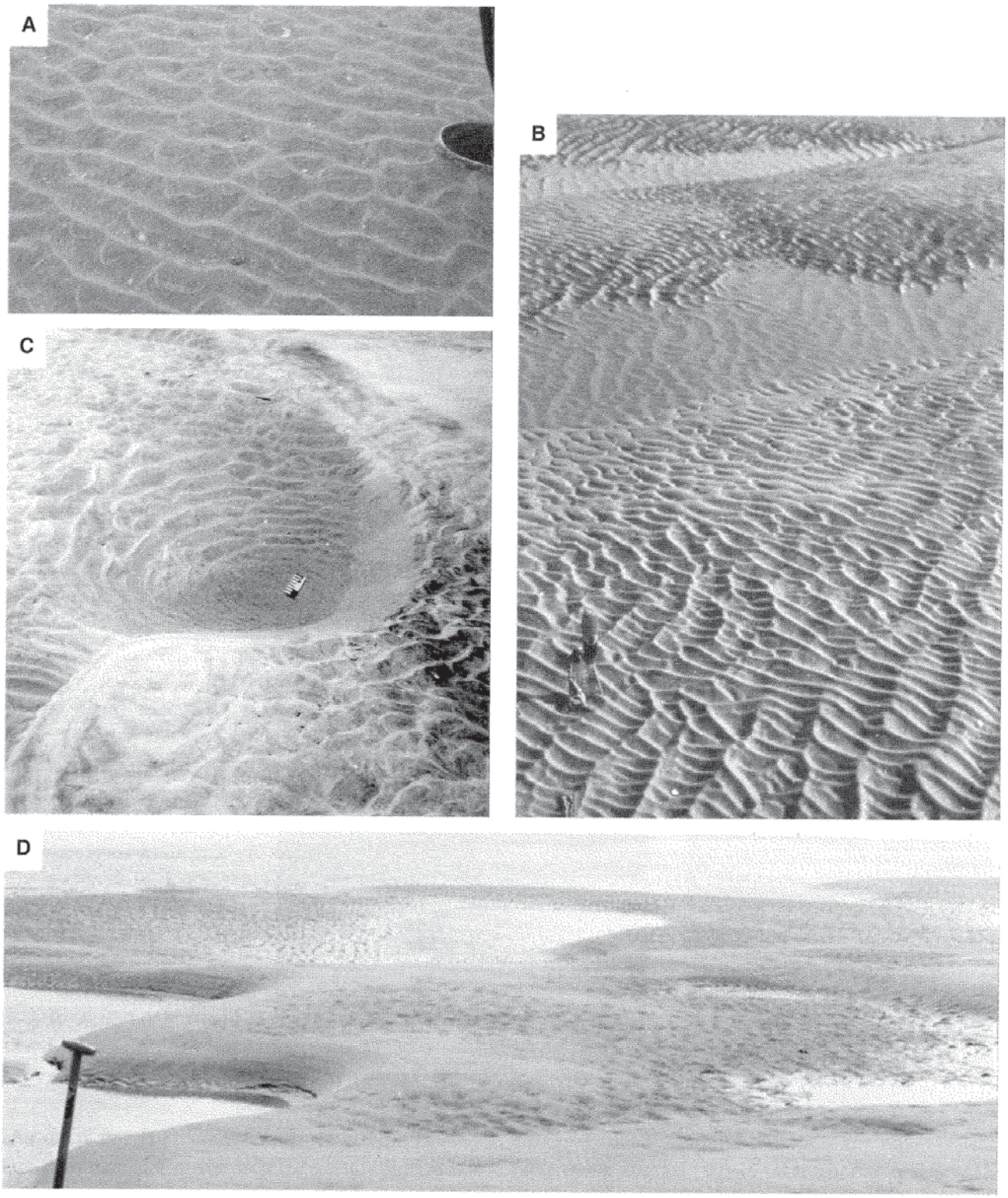

FIGURE 7.30. Bed forms associated with tidal currents. (A) Asymmetrical wave ripples modified by tidal sediment transport towards the observer. (B) Wave-ripple marks superimposed on tidal dunes, some of which have crests truncated by tidal flows. (C) An ebb-oriented tidal dune with a ripple fan in the trough. (D) Flood-oriented tidal dunes modified by falling water level.

pellets (Demicco, 1983). If the mud was deposited as sand, greater thicknesses could be deposited during a single tidal cycle. Such pelleted mud would be expected to be cross stratified.

Variation in the thickness of sand–mud couplets in heterolithic bedding has been related to variation in tidal current strength and deposition rate associated with periodic variations in tidal range, such as neap–

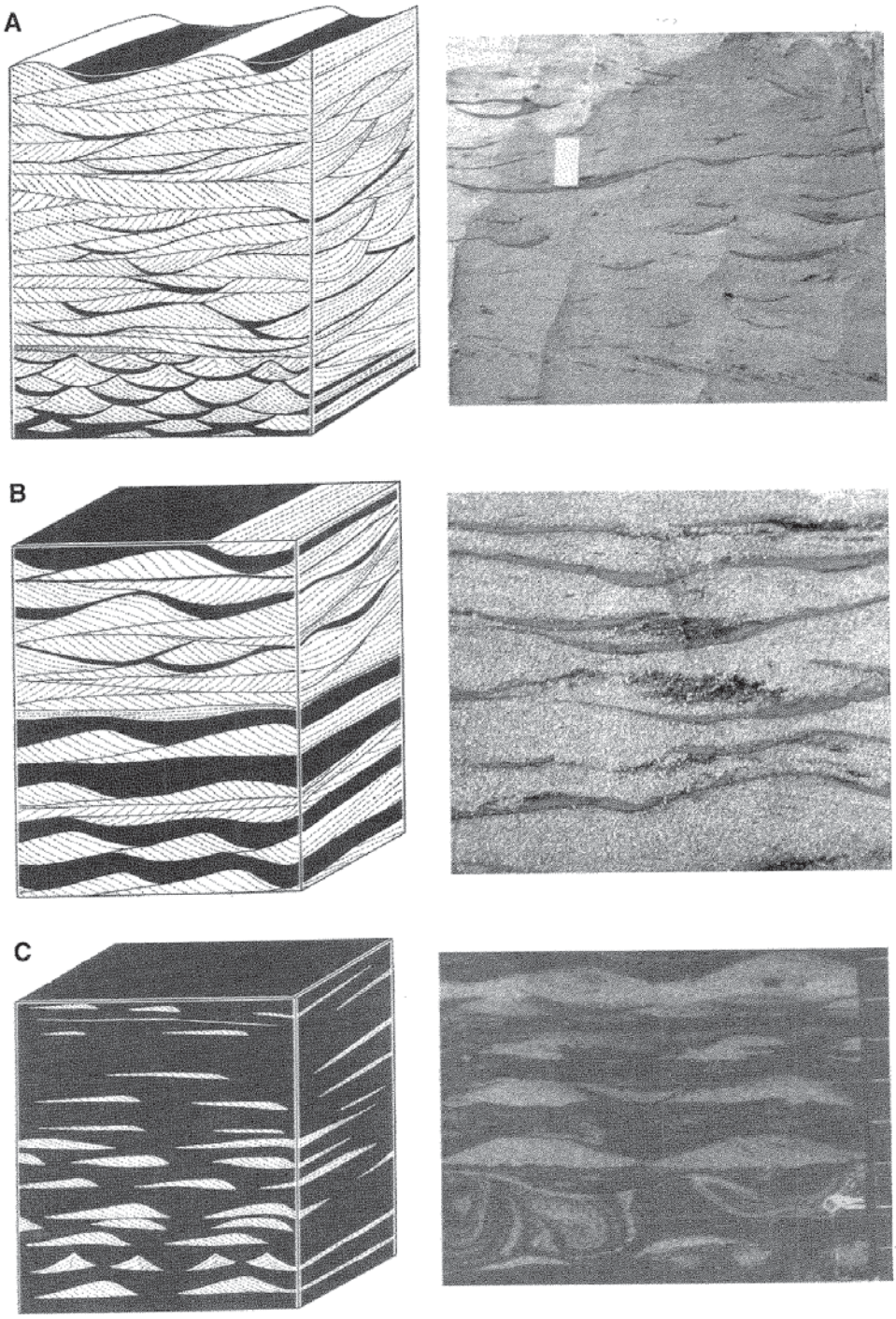

FIGURE 7.31. Flaser (A), wavy (B), and lenticular (C) bedding associated with current ripples, and symmetrical and asymmetrical wave ripples. From Reineck and Wunderlich (1968b). Mud is black, sand is white. Actual examples from North Sea tidal flats are shown to the right. Ripples are about 10 mm high.

spring cycles (as done for laminites). However, the relationship among tidal range, current speed, and deposition rate might not be straightforward, and variation in wind-wave currents may also have an influence (Terwindt, 1981; Nio and Yang, 1991).

Details of the spatial distribution of rippled sand and mud depend on the degree of asymmetry of the tidal currents, whether deposition occurred throughout the tidal cycle, and whether the depositional area is subjected to one (intertidal) or two (subtidal) slack water periods during a tidal cycle (Figures 7.26 and 7.31). If tidal currents are symmetrical and deposition occurs both during the ebb tide and during the flood tide, cross laminae in the sand would dip in opposing directions, and slackwater mud drapes would separate the ripples with opposing flow directions. If tidal currents are strongly asymmetrical, or deposition occurs only during the ebb or flood tide, the cross laminae would dip in one direction only, and the mud drapes would represent two slackwater periods and the subordinate tide (Figure 7.31). In subtidal settings, two slackwater mud drapes could occur during a single

tidal cycle, but only one could occur in intertidal settings.

Dunes

Dunes formed by tidal currents may have straight crestlines (2D) or curved crestlines (3D); for reviews of dune geometry see Allen (1982a) and Dalrymple and Rhodes (1995). They are commonly asymmetrical in along-stream section, and the degree of asymmetry varies with the asymmetry of the tidal currents. Most dunes will undergo some change in shape (in along-stream section) in response to changes in flow direction. Frequency distributions of dune height and wave length are commonly polymodal, and change with time as tidal currents change. This polymodality is partly due to the delayed response of dune height and length to changing flow conditions: dune lag (Allen, 1982a). Wave ripples and tidal current ripples are commonly superimposed on the surfaces of dunes during periods of low tidal current velocity (Figure 7.30).

Migration of tidal dunes generates medium-scale cross strata. Superimposed sets of medium-scale cross strata formed by tidal dunes (Figure 7.32) may indicate reversing flows if tidal currents were near symmetrical (*herringbone cross stratification*). Superimposed sets may also indicate flow in one direction if the tidal currents are strongly asymmetrical or if deposition from either asymmetrical or symmetrical tidal currents occurred only during the flood or ebb. Reactivation surfaces are common in cross sets formed by tidal dunes. Some of these are due to dunes overtaking each other, as is the case with dunes migrating under unidirectional flows. Other types of reactivation surfaces are formed by slackening and reversal of tidal currents. As the tidal currents slacken, ripples may form and migrate on the dunes. As tidal current speed further declines, wave ripples may form, if waves are active, or mud drapes may be deposited (Figure 7.32).

Characteristic patterns of stratification are formed by dune migration under symmetrical and asymmetrical tidal currents for the case when deposition occurs throughout the tidal cycle, and where sand and mud are available for transport; e.g., Allen (1985) (Figures 7.26 and 7.32). For strongly asymmetrical tidal currents, the dune migrates and forms medium-scale cross strata under the dominant tide. As the tidal current slackens, current and/or wave ripples may form on the dune, and finally a mud drape may be deposited, depending on whether the setting is intertidal or subtidal. During the subordinate tide, limited sand transport may occur as ripples, leaving a relatively thin deposit. Another mud drape may be deposited during the following slack-water period, depending on whether the setting is subtidal or intertidal. In the case of symmetrical tidal currents, dune migration is followed by ripple formation and (perhaps) mud-drape deposition both during ebb tide and during flood tide (Figure 7.32). The characteristic deposit formed during a single tidal cycle is referred to as a *tidal bundle*. Systematic variation in the thickness of tidal bundles has been related to variations in tidal range associated with neap–spring cycles and even the diurnal inequality of the tide (Figure 7.32) (Visser, 1980; Boersma and Terwindt, 1981; Terwindt, 1981; Allen, 1982b; Nio *et al.*, 1983; Allen and Homewood; 1984; Dalrymple, 1984; De Mowbray and Visser, 1984; Nio and Yang, 1991). The basis of this interpretation is that the thickness of a medium-scale cross stratum is related to the rate of dune migration, which is in turn related to the tidal current velocity and tidal range. It seems improbable that such a linkage could exist. For example, the dune-migration rate varies with dune height as well as with the sediment-transport rate. Nevertheless, cases of systematic thinning and thickening of sequences of 28 tidal bundles have been recorded, and an alternative explanation is not likely.

Tsunami

Tsunami (from Japanese *tsun* meaning harbor and *ami* meaning wave) are water-surface waves generated by a sudden change in the elevation of the ocean floor (related to earthquakes and landslides) that displaces overlying ocean water vertically. Such movement affects the whole water column in addition to the water surface. Volcanic eruptions and meteorite impacts can also displace water and generate tsunami. Tsunami waves travel rapidly across the ocean, and their amplitude increases near coasts, commonly being on the order of meters. At the coast, the waves surge inland with water velocities on the order of meters per second and depths of meters. Tsunami-wave surges can reach elevations of tens of meters above mean sea level up to a few kilometers inland. Although tsunami waves are particularly common in the Pacific Ocean, they affect all oceans to some degree. Tsunami can have a devastating effect on life and property (Figure 1.3A), and human death tolls from major tsunami are typically tens of thousands. Warning systems are in place, but not everywhere, and they are not always adequate. Tsunami waves are capable of

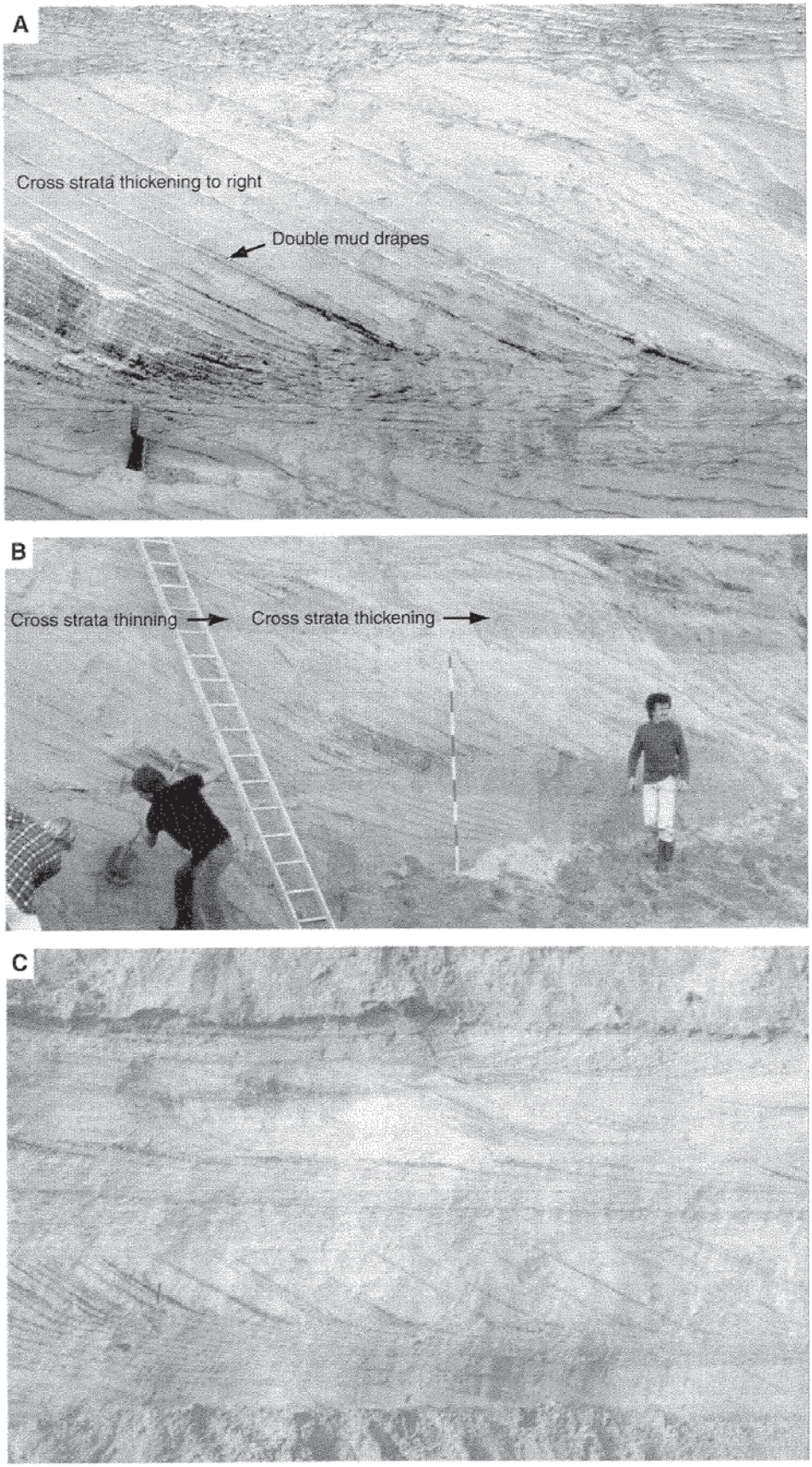

FIGURE 7.32. Cross strata due to tidal dunes: (A) and (B) tidal bundles with double mud drapes, and progressive thinning and thickening of cross strata associated with neap–spring tidal cycles, from subtidal channel deposits of the southwest Netherlands; and (C) tidal bundles and herringbone cross strata from subtidal channel deposits of the southwest Netherlands (photo from Janrik Van Den Berg).

performing significant erosion and deposition, particularly in coastal regions, and ancient sediments thought to be deposited by tsunami have been used to interpret past major earthquakes and meteorite impacts.

The tsunami that resulted from the Sumatra–Andaman earthquake of 26 December 2004 is undoubtedly the most damaging and best recorded in history up to this point (e.g., Lay *et al.*, 2005; Moore *et al.*, 2006). More than 283,000 people died, and millions more were rendered homeless. Numerous investigations of the nature of this earthquake and tsunami, and the impact of the tsunami on humans and the Earth's surface are under way, and these will be published in due course. Some of the preliminary information is included below.

Tsunami generation

Over the past 150 years, one to two tsunami have occurred per year on average, and more than 80% of these have been caused by submarine earthquakes. Most submarine earthquakes are not large enough to generate tsunami, and earthquakes with Richter magnitudes greater than 7 cause most tsunami. However, earthquakes of lower magnitude can generate tsunami if they initiate subaqueous landslides. Subduction zones are the prime sites for large-magnitude earthquakes, and these can be associated with ruptures of the ocean floor with vertical movements of meters and lengths of hundreds of kilometers, involving areas of up to 10^5 km^2 and volumes of rock of up to 10^3 km^3. Tsunami-wave amplitude (at the source and at some distant coast) increases with the volume of the displaced rock and with the magnitude of the earthquake (Bryant, 2001). The shapes of tsunami waves are quite variable at the point of generation, depending on the distribution of uplift and subsidence, and propagate at right angles to the rupture orientation (Figures 7.33 and 7.34).

The main shock of the Sumatra–Andaman earthquake of 26 December 2004 had a Richter magnitude of between 9.1 and 9.3, and was followed by many aftershocks with magnitudes in excess of 5 (Lay *et al.*, 2005). The earthquake was due to fault slip associated with the subduction zone separating the Indo-Australian and SE Eurasian plates. The fault slip occurred over a length of more than 1300 km, extending from NW Sumatra northwards to the Andaman Islands (Figure 7.35). The width of the faulted zone was up to about 240 km, and faulting occurred over a depth

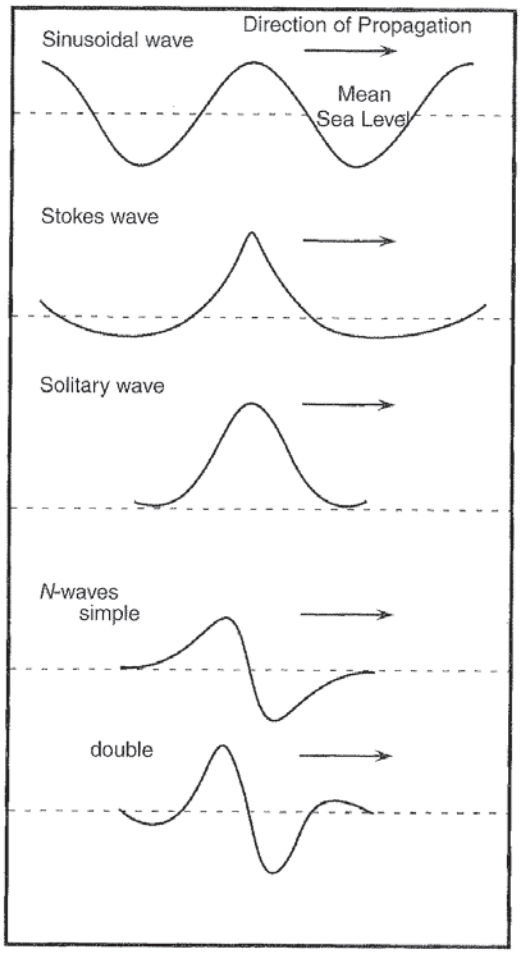

FIGURE 7.33. Idealized cross profiles of tsunami waves. From Bryant (2001).

of 30–45 km. The epicenter of the earthquake was just offshore and to the west of NW Sumatra (Figure 7.35), and the rupture propagated to the north, as recorded by aftershocks. The amplitude, propagation velocity, and duration of the fault slip varied in space and time. Slippage lasted for at least 500 seconds, and was up to 15 m near Banda Aceh.

Landslides can involve displacement of similar areas and volumes of rock or sediment to those displaced by earthquake ruptures. Earthquakes can, of course, initiate landslides, especially on the steep slopes of oceanic trenches and continental margins, but so can eruptive activity on the slopes of volcanoes. The character of tsunami waves generated by landslides depends on their volume, the flow depth, and the rate of movement. The lengths and periods of the initial waves (typically on the order of kilometers and minutes, respectively) are less than those generated by earthquakes (typically on the order of tens to hundreds of kilometers and minutes to tens of minutes, respectively), and the wave profile is typically N-shaped (Figure 7.33).

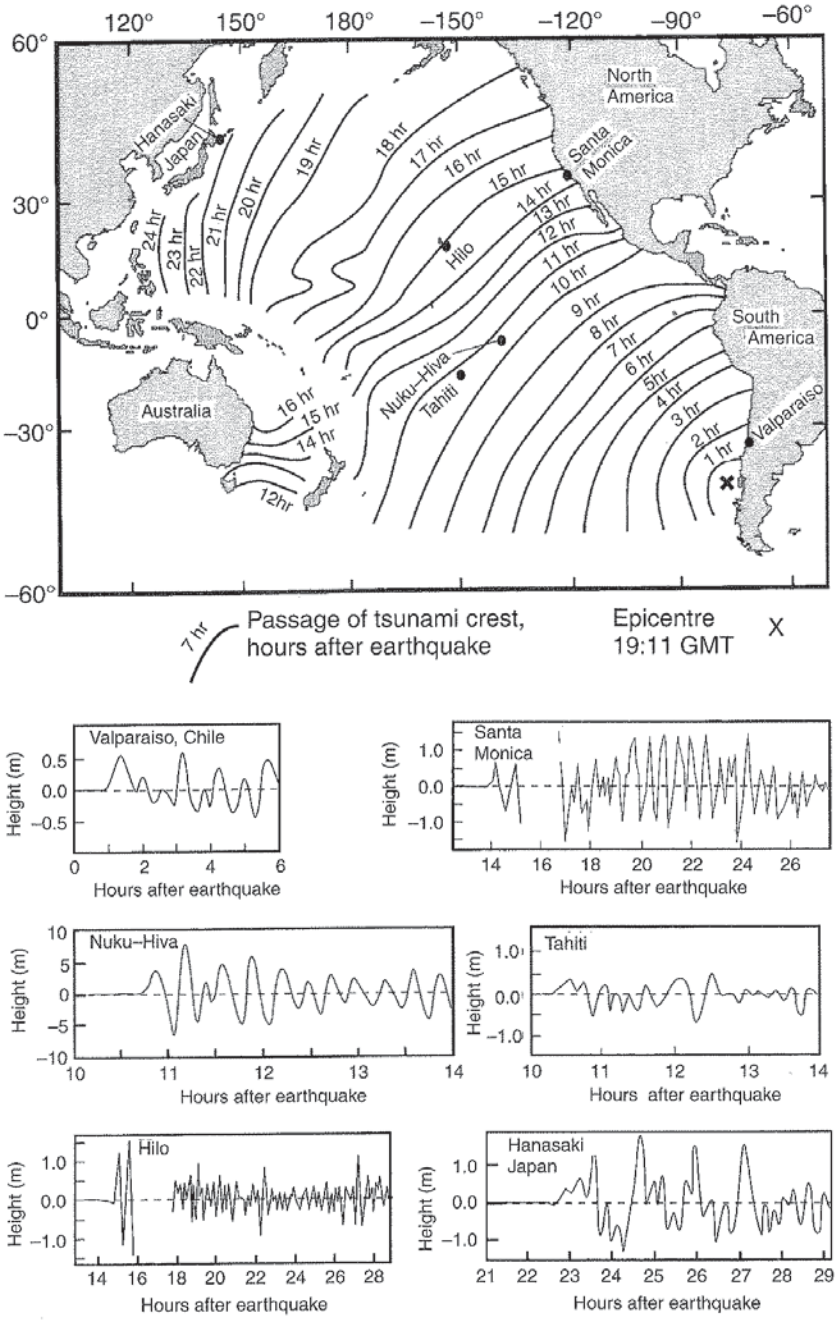

FIGURE 7.34. (A) Passage of a tsunami wave crest across the Pacific Ocean following the 22 May 1960 Chilean earthquake, and (B) water-level records at selected stations (daily tides removed). From Bryant (2001).

Tsunami waves associated with volcanic eruptions can be generated by earthquakes, landslides, submarine eruptions, subaerial flows of ash or lava into the sea, and collapse of volcanoes to form calderas. Spectacular examples include Krakatoa (1883), Pelee (1902), and Santorini (1650 BC). Ancient meteorite impacts have been inferred to generate tsunamis, and these inferences have been based on preserved sediment deposits (e.g., Bourgeois *et al.*, 1988) and computer simulations (Hills and Mader, 1997; Crawford and Mader, 1998). Figure 7.36 shows predictions of the height of tsunamis as a function of meteorite diameter, impact velocity, and distance from the impact.

Tsunami dynamics

The shapes, periods, and current velocities associated with tsunami waves are recorded by tide gauges, buoys and various other tethered instruments throughout the oceans, and satellite altimetry. The Deep Ocean Assessment and Reporting of Tsunamis (DART) Project is a U.S. National (NOAA) effort to maintain and improve the capability for the early detection and real-time reporting of tsunamis in the open ocean. The DART systems consist of an anchored sea-floor pressure recorder and a companion moored surface buoy for real-time communications. Data from the sea-floor

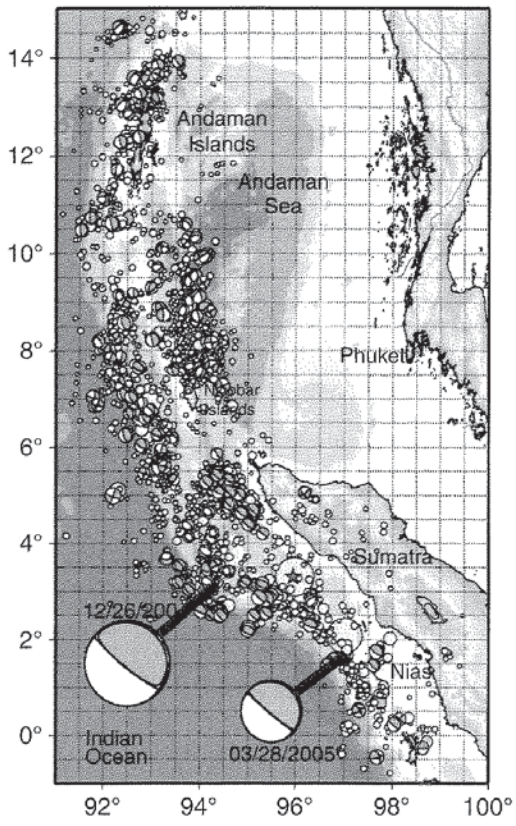

FIGURE 7.35. A map showing aftershock locations (circles with diameter proportional to seismic magnitude) for 13 weeks after the 26 December 2004 Sumatra–Andaman earthquake. From Lay *et al.* (2005). The epicenter is shown by a star within a large circle. The spatial distribution of aftershocks outlines the area of fault slip.

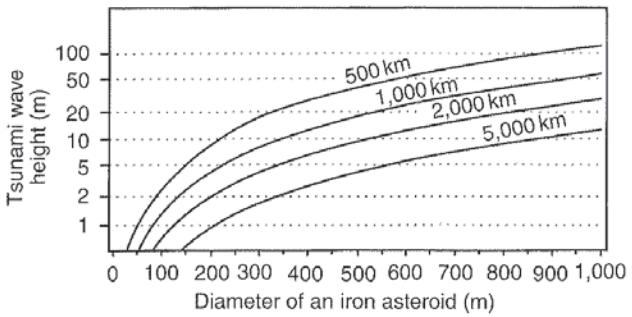

FIGURE 7.36. Predictions of the height of tsunamis as a function of meteorite diameter, impact velocity, and distance from the impact. From Bryant (2001).

recorder are transmitted acoustically to the surface buoy, and then relayed via satellite to ground stations.

Most waves generated by large earthquakes are sinusoidal waves with heights normally less than a meter, lengths of 10–500 km, and periods of 100–2000 s. Several waves are normally generated, and the position of the largest wave in the train is variable. These waves can be considered to be Airy shallow-water waves (wave length/water depth > 20) in water depths greater than a few tens of meters, because they have small amplitude and great length relative to the water depth. The celerity of Airy shallow-water waves decreases as the square root of depth (Equation (7.7)), and wave speeds (celerities) are typically 160–250 $m\,s^{-1}$ in the open ocean, 30–85 $m\,s^{-1}$ on continental shelves, and on the order of 10 $m\,s^{-1}$ near the coast (Bryant, 2001). As such waves propagate away from the generation area, the long-period waves travel faster than do waves of shorter period (wave dispersion) such that the long waves reach coastlines first. Over long-distance travel, wave paths must be corrected for geometric spreading on a spherical surface.

Important transformations of Airy waves occur as they move into shoaling water and become more influenced by the bed, as discussed above. The waves become increasingly peaked (trochoidal), asymmetrical in profile, higher, and shorter. They change from Airy waves to Stokes waves. Some waves become solitary waves or N-shaped waves (Figure 7.33). Instead of water particles beneath the waves following closed circular orbits, the orbits become increasingly elliptical and unclosed. This results in net drift of near-bed fluid in the direction of wave propagation, but in the opposite direction nearer the water surface. The maximum near-bed orbital velocity is given approximately by Equation (7.11). Maximum velocities near coasts are typically 2–4 $m\,s^{-1}$, which is similar to the velocity of large storm waves.

As shallow-water waves move over sea-bottom topography, especially that associated with coasts, they are refracted (due to variation of wave speed with depth). Wave diffraction occurs as waves pass through narrow spaces between land areas such as islands. Tsunami waves are always reflected at the coast, irrespective of bed slope and wave height. This means that edge waves should also be present. Resonant amplification of reflected waves, and of edge waves and incoming waves, means that wave heights will vary substantially along a coastline, and the highest wave at the coast may end up not being the largest incoming wave. Resonant amplification can double the height of an incoming wave.

The geometry and water motions of tsunami waves can be modeled numerically using the Navier–Stokes equations for low-height, long waves, considering also friction at the bed and the Coriolis force (e.g., Mader, 1974, 1988; Satake, 2005). The equations are solved using nonlinear, finite-difference methods using variable grid sizes and shapes. This requires detailed knowledge of the bed topography. Figure 7.37 shows one of

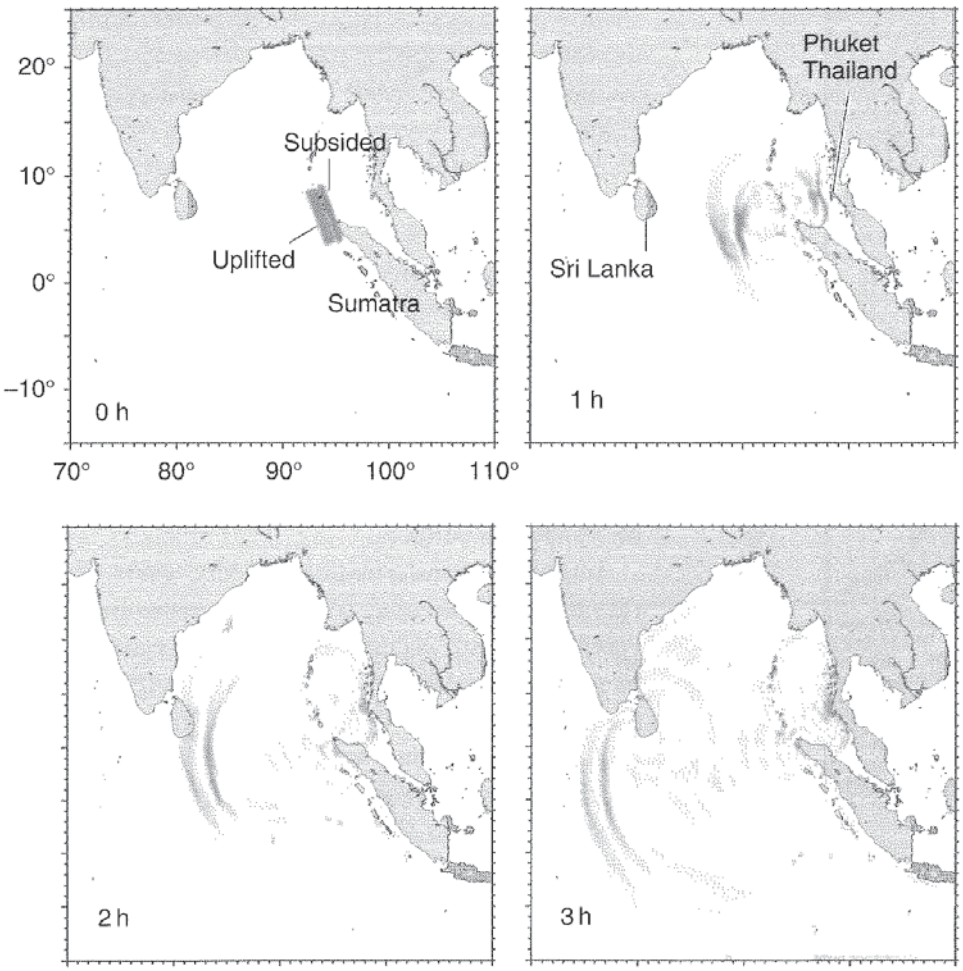

FIGURE 7.37. Numerical simulation of tsunami wave motions following the Sumatra–Andaman earthquake (from an animation available at http://staff.aist.go.jp/kenji.satake/animation.gif). Dark areas are amplitude highs, with darkness increasing with wave amplitude.

several simulations of tsunami-wave motion for the Sumatra–Andaman tsunami. Accurate simulations can be produced within hours of tsunami initiation.

Tsunami waves tend to surge up the shore rather than to break. The surge of a tsunami wave can move inland for distances of hundreds of meters to kilometers, and reach elevations that exceed the maximum water level at the coast by a factor of two or more (meters to tens of meters). The distance inland reached by the run-up increases with the water level at the coast, and decreases with the flow resistance (bed roughness). With the 2004 Sumatra–Andaman tsunami, the surging water in Sumatra traveled inland for up to kilometers, and the water depth of the surge at Banda Aceh exceeded 20 m with run elevations in excess of 35 m (Moore *et al.*, 2006). If the depth of surging water is similar to the wave height at the coast, run-up velocities are typically meters per second, and return flows are probably faster. The water-surface slope is typically on the order of 0.001. Run-up height, length, and flow velocity can be predicted accurately by numerical solution of the shallow-water, long-wave equations.

Sediment transport, erosion, and deposition associated with tsunami

Much of what is known about water flow, sediment transport, erosion, and deposition associated with tsunami is inferred, because scientists have been reticent about making measurements during tsunami activity. Flow velocities of near-bed currents near the coast and during run-up on the land are expected to be meters per second, comparable to those of large storm waves. These flows are capable of moving gravel-sized sediment (even boulders up to meters across) on the bed, and sand-sized sediment and finer in suspension. The bed forms expected under these conditions are a near-plane bed or dunes with lengths of tens of meters and heights up to meters (Chapter 5), as long as there is sufficient time to form them. The time of action of these currents is on the order of minutes (compared with seconds for storm waves), but this might not be enough time to form dunes. Tsunami surges are also capable of causing great destruction to buildings, animals, and vegetation, due not only to the force of the moving water but also to the hard objects carried by the flow. Tree trunks are

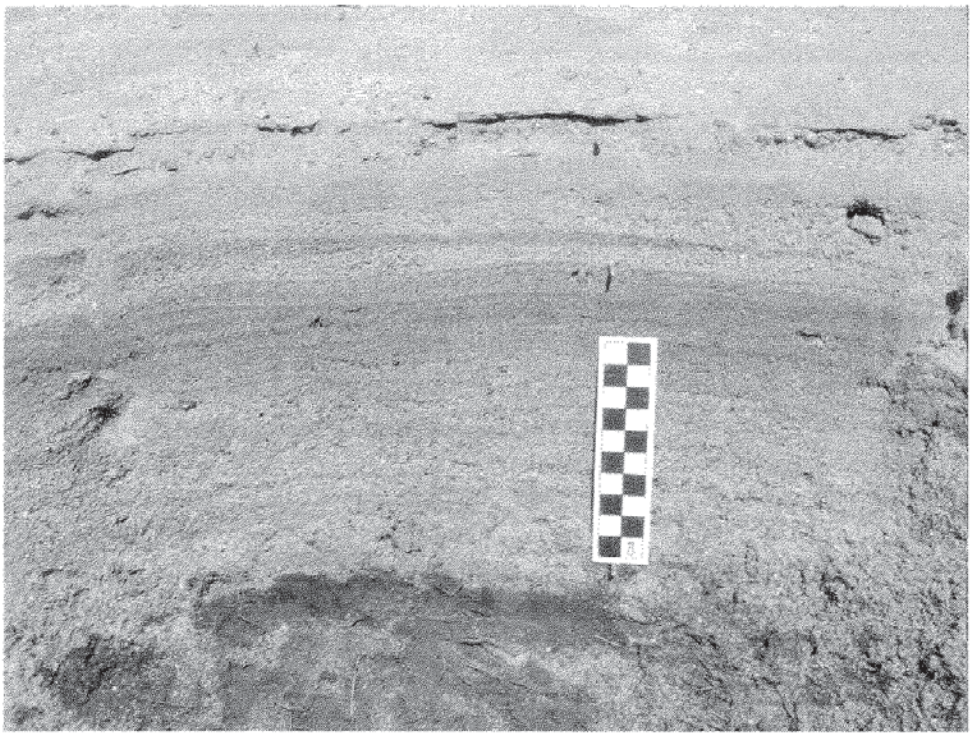

FIGURE 7.38. A 2004-tsunami deposit from Banda Aceh, Sumatra. Photo courtesy of Guy Gelfenbaum of the US Geological Survey (http://walrus.wr.usgs.gov/tsunami/sumatra05/).

readily snapped off near their bases by tsunami waves, and debarked by "tools" carried by the flow.

Erosion and deposition of sediment requires along-stream increases or decreases in flow velocity and sediment-transport rate. The most common type of deposit attributed to tsunami in coastal settings is a sheet of sand up to about 0.5 meters thick that thins in the landward direction (e.g., Dawson *et al.*, 1991; Shiki *et al.*, 2000; Bryant, 2001) (Figure 7.38). The sand overlies coastal mud, soil, or peat with a sharp base. Erosion of underlying material is suggested by the presence of rip-up clasts. The deposit may contain wood, leaves, and marine fossils such as large shells, foraminifera, and diatoms. The mean grain size commonly decreases upwards and landwards. Large isolated clasts up to boulder size can occur in these deposits. There is little information about the internal structure of these deposits, although diffuse planar laminae have been recorded. A lack of internal structures suggests rapid deposition from suspension. A series of stacked fining-upward units has been interpreted as deposits of individual waves comprising one tsunami event. However, there is no reason to suppose that each wave will deposit a fining-upward layer. The sharp tops of some units have been interpreted as due either to backwash or to the passage of a later wave. Attempts have been made to interpret tsunami-wave characteristics from the thickness and grain size of tsunami sand layers, using theoretical models. However, such approaches are not well developed, and a comprehensive sediment-routing model (Chapter 5) has not been used for this purpose.

In the case of the 2004 Sumatra–Andaman tsunami at Banda Aceh, erosion occurred near the coast, but deposition occurred further landwards, as far as the inundation (Moore *et al.*, 2006). Buildings, soil layers, and trees were eroded. The deposit is generally 5–20 cm thick, but locally reaches 80 cm, and tends to fill low spots (Figure 7.38). The deposit is very coarse to medium sand, decreasing in grain size upwards and landwards. In some places, up to three distinct layers can be discerned, indicating deposition from discrete waves. The sand is either structureless or planar laminated. Larger clasts of soil, coral, and concrete also occurred. Further from shore, broken trees and contents of buildings form a larger part of the deposit.

Tsunami sand deposits are very difficult to distinguish from sand deposited by a storm-surge washover (Tuttle *et al.*, 2004; Chapter 15). Storm surges produce only one depositional unit at a time, but it is common for units deposited at different times to be superimposed. Although multiple fining-upward units in supposed tsunami deposits might be formed by different waves in one event, they could also be formed by different events. It is also difficult to date ancient deposits accurately enough to link them to a specific event, whether it is a tsunami or a major storm surge. Large lateral extent is commonly cited as evidence for tsunami deposits, but the lateral extents of storm-surge washovers can be comparable.

Despite the uncertainties in the unambiguous recognition of ancient tsunami deposits, such interpretations have been used to infer the nature of ancient earthquakes (e.g., Atwater and Hemphill-Haley, 1997; Shiki *et al.*, 2000; Atwater *et al.*, 2005; Bondevik *et al.*, 2005; Rhodes *et al.*, 2006).

Other coastal deposits attributed to tsunamis are dunes in sands and gravels with heights of meters and lengths of tens to hundreds of meters, and chenier-like ridges of shell-rich sand with similar dimensions to dunes. Mounds of unsorted sediment (diamictons) also occur, although their origin is uncertain. Isolated boulders or clusters of imbricated boulders occur at the base of cliffs or marking swash lines. Boulders that are 1–4 m across require flow velocities of 5–10 $m\,s^{-1}$ to move them. It has also been claimed (Bryant, 2001) that many large-scale depositional features of coastlines such as overwash fans, barrier beaches, and flood-tidal deltas might owe their origin to tsunamis. Although tsunamis might influence the form of such features, the minutes of tsunami flow are surely not long enough to effect a great deal of deposition, and episodic deposition by storm waves over many years is more likely.

In deeper marine environments, deposits of sediment gravity flows (Chapter 8) have been associated with earthquakes, and related also to tsunamis (e.g., Pickering *et al.*, 1991). The sediment gravity flows might have been initiated either by earthquakes, or by the cyclic wave loading of sediment by the tsunami waves. Sediment-gravity-flow deposits have also been related to tsunamis supposedly generated by meteorite impacts (e.g., Bourgeois *et al.*, 1988). However, exceptional sediment-gravity-flow deposits are not necessarily initiated by tsunamis. We conclude that interpretation of ancient deposits as due to tsunamis is far from clear cut, since there are normally other possible origins.

Erosional features in bedrock that have been attributed to tsunamis are pits, grooves, flutes, and potholes that could be formed by cavitation, and impacts and abrasion by moving grains (Bryant, 2001). Loose-joint blocks can also be moved from cliffs by high dynamic pressures, and either fall to the base of the cliff or are transported by the flow. None of these processes is unique to tsunami (see the discussion of erosion of bedrock coastlines in Chapter 15). The occurrence of such features well above normal high water level has been used to justify a tsunami origin. However, these features could be formed by storm waves acting during a previous period of higher relative sea level. Furthermore, it is unlikely that major erosion of bedrock could occur during the minutes that water flows during a tsunami. Erosion of bedrock requires many years of pounding by water and sediment.